

WIMP-FIMP option and neutrino masses via a novel anomaly-free $B - L$ symmetry

Sarif Khan^{1,*} and Hyun Min Lee^{1,†}

¹*Department of Physics, Chung-Ang University, Seoul 06974, Korea.*

Abstract

We propose a novel $U(1)_{B-L}$ model with singlet dark matter fermions composed of WIMP and FIMP, which is anomaly-free without a need for introducing right-handed neutrinos. Fermion dark matter masses are generated after the $U(1)_{B-L}$ is broken spontaneously, so the Yukawa couplings for WIMP and FIMP components can be distinguished by the hierarchical values of the vacuum expectation values of the single scalar fields. Moreover, the $U(1)_{B-L}$ gauge boson receives a TeV-scale mass for a tiny extra gauge coupling, so it goes out of equilibrium from the rest of the model content in the early Universe. Both the $U(1)_{B-L}$ gauge boson and FIMP component are produced from the decays of the bath particles, and the former can decay into FIMP DM and/or WIMP DM before BBN. The WIMP component can reside in the resonance region of the Higgs bosons or dominantly annihilate into a pair of singlet-like scalars. Thus, there is a flexibility to choose a small mixing between the visible and dark sectors, thereby evading all the current direct and indirect detection bounds. Furthermore, we show that WIMP and FIMP components can coexist in suitable fractions, depending on the choice of model parameters, allowing for additional protection for WIMP DM against various experimental bounds. Finally, we identify the dimension-6 and dimension-7 operators for Majorana neutrino masses in our model, being consistent with the $U(1)_{B-L}$ gauge symmetry, and provide a possibility of extending the model with additional singlet fermions for neutrino masses.

*Electronic address: sarifkhan@cau.ac.kr

†Electronic address: hminlee@cau.ac.kr

I. INTRODUCTION

When dark matter (DM) mostly self-annihilates into the Standard Model (SM) sector, most of the parameter space for the so-called Weakly Interacting Massive Particle (WIMP) has been explored with the increased detector volume and state-of-the-art DM detection techniques. However, there is no evidence for the DM interactions with the SM apart from gravitational interaction. So far, the experiments have looked for DM with a weak coupling to the SM, but with null results. For instance, the recent data from LUX-ZEPLIN [1] have ruled out the spin-independent direct detection (SIDDD) cross-section up to $\sigma_{SI} \sim 10^{-48}$ cm² for a DM mass of about 50 GeV. With such a severe bound, Higgs portal DM can only survive near the resonance region. Therefore, we need to consider different kinds of DM candidates with weaker couplings to the SM or go beyond the standard scenarios such as WIMP DM annihilating into an additional dark sector.

There are still many possibilities to overcome the SIDDD bounds and open up larger parameter spaces that have not been explored yet. One popular alternative to evade these bounds is the freeze-in DM scenario [2, 3], referred to in the literature as Feebly Interacting Massive Particle (FIMP), where the coupling strength is so tiny that freeze-in DM is very difficult to probe in ongoing experiments. Another possibility is multi-component DM [4–9], which is very well motivated because our visible world consists of many particles, from quarks/leptons to gauge bosons as force carriers. In the case of multi-component DM, we can consider scenarios with both WIMP-type DM, both FIMP-type DM or a combination of WIMP and FIMP DM. For multicomponent WIMP DM, one WIMP DM candidate could annihilate into another WIMP DM candidate, and the second WIMP DM candidate could annihilate into the visible sector. By suitably choosing the fraction of the second WIMP DM candidate, we can always evade the existing bounds, and the freeze-out mechanism will practically remain effective for a longer time, even if the DD experiments reach the neutrino floor [10]. As discussed, it is challenging to detect FIMP DM, but a detectable FIMP DM can be achieved, with an appropriate adjustment of the reheating temperature [11–14].

In this article, we explore the possibility of WIMP and FIMP DM and search for the parameter space that has not been explored by any experiments. To this purpose, we consider a well-known $U(1)_{B-L}$ gauge extension of the SM, but without three right-handed neutrinos which used to be required to cancel the gauge anomalies [15]. The main disadvantage of $U(1)_{B-L}$ gauge symmetry with right-handed neutrinos [16–20] is that there is no suitable candidate for DM unless one of the right-handed neutrinos is detached from the visible sector through the symmetry or it is assumed to have tiny interactions with the visible sector [4].

In our work, we introduce four additional chiral fermions [21, 22] with suitable charges to cancel the gauge anomalies arising from $[SM]^2 \times U(1)_{B-L}$ and $[U(1)_{B-L}]^3$. In Refs. [21, 22], the

authors studied single-component WIMP DM¹ near the resonance region. In the present work, we explore a multi-component DM consisting of WIMP and FIMP combinations.

To cancel the gauge anomalies introduced by $U(1)_{B-L}$, the SM is extended with four chiral fermions, comprising two left-handed and two right-handed fermions with fractional charges, along with two singlet scalars. One CP-odd scalar *d.o.f.* among the two becomes the longitudinal component of the additional $U(1)_{B-L}$ gauge boson, rendering it massive, while the other becomes a physical CP-odd particle that actively participates in the DM phenomenology [23].

In the present model, there are three CP-even scalars: two arising from the singlet scalars and one from the SM Higgs doublet. All three scalars contribute to the DM phenomenology. The $U(1)_{B-L}$ charge assignments of the singlet scalars are made such that two Dirac fermions can be realized from the four chiral fermions. Both Dirac fermions act as DM candidates, with one being of the WIMP type (ψ_1 , as defined in Section II) and the other of the FIMP type (ψ_2 , as defined in Section II). Moreover, we take the mixing among two Dirac fermions to zero by making the associated Yukawa couplings to zero or introducing two independent Z_2 symmetries. The distinction between the couplings for WIMP and FIMP DM arises from the hierarchy between the VEVs of the singlet scalars, v_1 and v_2 , namely, $v_1 \gg v_2$. However, in the scenarios where $v_1 \sim v_2$ and $v_{1,2} \sim \mathcal{O}(\text{TeV})$, both DM candidates are of the WIMP type, whereas for $v_{1,2} \sim \mathcal{O}(\text{PeV})$, both are of the FIMP type. We consider a GeV-scale mass for the Z_{BL} gauge boson, which places the extra gauge coupling g_{BL} in the feeble regime for a PeV-scale VEV of ϕ_1 . In the presence of such a feeble coupling rendering Z_{BL} non-thermal, we determine the non-thermal distribution for Z_{BL} from the first principles and compare it with the results that would have been obtained with a thermal distribution.

In the case of WIMP-type DM, aside from the Higgs resonance region, there is a large parameter space where DM predominantly annihilates into BSM scalars. This provides the freedom to arbitrarily choose the mixing angle between the visible and dark sectors, effectively evading the existing bounds for WIMP DM. On the other hand, for FIMP-type DM candidates, we primarily consider the decay modes for DM production, which dominate over the annihilation contributions.

In our study, we include all the relevant constraints on the model, such as perturbativity bounds, vacuum stability bounds, Higgs measurements, direct detection, indirect detection, oblique parameters, and Big Bang nucleosynthesis (BBN). Moreover, we also consider higher dimensional operators for Majorana neutrino masses being consistent with the $U(1)_{B-L}$ symmetry. We consider the possibility of realizing such higher dimensional operators by introducing

¹ In Ref. [21], one of the extra Dirac fermions and beyond SM scalars were considered heavy and did not contribute to the DM phenomenology. In contrast, our study considers the full particle setup in the DM phenomenology.

three right-handed fermions with suitable charges while keeping the gauge anomalies cancelled and letting them interact with lepton doublets.

The rest of the paper is organized as follows. In Section II, we describe our model in detail. Section III discusses all the constraints associated with our study. In Section IV, we present our findings on DM. Finally, in Section V, we conclude our work. There is one appendix containing the analytical formulas for decay widths and collision terms, used in our study.

II. THE MODEL

We present the model setup in the extension of the SM with the $U(1)_{B-L}$ gauge symmetry. In this section, we discuss the conditions for gauge anomalies in our model and the mass spectrum and the mixing angles in the scalar sector after the $U(1)_{B-L}$ symmetry is broken. In the basis for physical fermions and scalars, we obtain the mass spectrum for singlet fermions and their interaction terms. We also show how neutrino masses are obtainable in the effective theory with $U(1)_{B-L}$ and the extension with three right-handed neutrinos.

Gauge	Quarks			Leptons		Higgs doublet
Group	$Q_L^i = (u_L^i, d_L^i)^T$	u_R^i	d_R^i	$L_L^i = (\nu_L^i, e_L^i)^T$	e_R^i	ϕ_h
$SU(2)_L$	2	1	1	2	1	2
$U(1)_Y$	1/6	2/3	-1/3	-1/2	-1	1/2
$U(1)_{B-L}$	1/3	1/3	1/3	-1	-1	0

Table I: Charge assignments for the SM matter content under the SM and $U(1)_{B-L}$ gauge groups.

The complete Lagrangian takes the following form,

$$\mathcal{L} = \mathcal{L}_{SM} + \sum_{i=1,2} (D_\mu \phi_i)^\dagger (D_\mu \phi_i) + \mathcal{L}_{BL}^{Kin} - \mathcal{V}(\phi_h, \phi_1, \phi_2). \quad (1)$$

On the other hand, the kinetic terms and the Yukawa terms for the additional fermions can be written as follows,

$$\begin{aligned} \mathcal{L}_{BL}^{Kin} = & \sum_{X=\xi_{1L}, \xi_{2L}, \xi_{1R}, \chi_{2R}} \bar{X} i \not{D} X + \alpha_1 \bar{\xi}_{1L} \chi_{1R} \phi_2 + \alpha_2 \bar{\xi}_{2L} \chi_{2R} \phi_1 + \beta_1 \bar{\xi}_{2L} \chi_{1R} \phi_1 \\ & + \beta_2 \bar{\xi}_{1L} \chi_{2R} \phi_2 + h.c. \end{aligned} \quad (2)$$

where $\not{D}X \equiv \gamma^\mu D_\mu X$. The covariant derivatives are $D_\mu X = \partial_\mu X - i g_{BL} n_{BL}^X Z_{BL} X$ where g_{BL} is the gauge coupling, n_{BL}^X is the $U(1)_{B-L}$ charge of the field X , as shown in Tables I and II, and Z_{BL} is the gauge field of the $U(1)_{B-L}$ symmetry.

Gauge Group	Extra fermions				Extra scalars	
	ξ_{1L}	ξ_{2L}	χ_{1L}	χ_{2L}	ϕ_1	ϕ_2
$SU(2)_L$	1	1	1	1	1	1
$U(1)_Y$	0	0	0	0	0	0
$U(1)_{B-L}$	a	b	c	c	n	$2n$

Table II: Charge assignments for extra fermions and scalar fields under the SM and $U(1)_{B-L}$ gauge groups.

From the Lagrangian in Eq. (2), we have the possibility to explore many types of DM scenarios by choosing different values for $\alpha_{1,2}$ and $\beta_{1,2}$. First, if we have $\alpha_{1,2} \sim \beta_{1,2} \sim \mathcal{O}(0.1)$, we can realize one or two-component WIMP-type DM, depending on whether the decay of one to another is open. The recent direct detection bound from LUX-ZEPLIN [1] has tightly constrained the parameter space for WIMP-type DM candidates if they dominantly annihilate into the SM sector. On the other hand, if we consider $\alpha_{1,2} \sim \beta_{1,2} \sim \mathcal{O}(10^{-10})$, then we can have FIMP-type DM candidates, which will be safe from all kinds of bounds but would be hardly probed in the near future with the ongoing experiments. The aforementioned Yukawa couplings for WIMP and FIMP type DM can be taken for $v_{1,2}$ of TeV and PeV scales, respectively, for GeV scale DM masses.

In the following discussion, we focus on a combination of WIMP and FIMP-type DM candidates, which remain safe from all the existing bounds while being detectable in the ongoing experiments. Additionally, due to the rich particle content, we can have a regime where WIMP-type DM mainly annihilates into the dark sector, i.e., singlet-like scalars. This gives us the freedom to choose the mixing angle between the dark sector and the visible sector freely without affecting the DM production, allowing us to evade all the terrestrial bounds. Therefore, in the present work, we consider $\alpha_1 \sim \mathcal{O}(0.1)$ and $\alpha_2 \sim \mathcal{O}(10^{-10})$, which can be easily achieved by choosing hierarchical² VEVs, $v_1 \gg v_2$. We can ensure the stability for the two-component DM scenario either by introducing two independent $Z_2 \times Z'_2$ symmetries for WIMP and FIMP or by taking $\beta_{1,2} = 0$ in Eq. (2) (or zero mixing angles between the singlet fermions, i.e. $\theta_{L,R} = 0$, defined in Eq. (16)).

² In the literature, hierarchical VEVs between scalar multiplets under the same gauge group have been considered for obtaining suitable phenomenology, *e.g.*, in the Type II seesaw mechanism [24, 25], where one can take the triplet scalar VEV to the eV scale, leading to the doubly charged Higgs predominantly decaying into two leptons [26, 27].

The scalar potential for the SM Higgs doublet and two singlet scalars obeying the complete gauge symmetry takes the following,

$$\begin{aligned}
\mathcal{V}(\phi_h, \phi_1, \phi_2) = & -\mu_h^2 \left(\phi_h^\dagger \phi_h \right) + \lambda_h \left(\phi_h^\dagger \phi_h \right)^2 - \mu_1^2 \left(\phi_1^\dagger \phi_1 \right) + \lambda_1 \left(\phi_1^\dagger \phi_1 \right)^2 - \mu_2^2 \left(\phi_2^\dagger \phi_2 \right) \\
& + \lambda_2 \left(\phi_2^\dagger \phi_2 \right)^2 + \lambda_{h1} \left(\phi_h^\dagger \phi_h \right) \left(\phi_1^\dagger \phi_1 \right) + \lambda_{h2} \left(\phi_h^\dagger \phi_h \right) \left(\phi_2^\dagger \phi_2 \right) \\
& + \lambda_{12} \left(\phi_1^\dagger \phi_1 \right) \left(\phi_2^\dagger \phi_2 \right) + \mu \left(\phi_2 \phi_1^\dagger + \phi_2^\dagger \phi_1 \right)
\end{aligned} \tag{3}$$

A. Gauge anomalies

In the present work, we have introduced singlet fermions, which are charged under the $U(1)_{B-L}$ gauge symmetry. We have chosen the charges of such singlet fermions in such a way that they make non-trivial contributions to $[U(1)_{B-L}]^3$ and $[\text{Gravity}]^2 \times U(1)_{B-L}$. Moreover, we also have constraints on the charges of the particles involved in the Yukawa terms. Therefore, the constraints can be summarised in the following manner,

$$\begin{aligned}
[U(1)_{B-L}]^3 & \rightarrow a^3 + b^3 - 2c^3 = 3, \\
[\text{Gravity}]^2 \times U(1)_{B-L} & \rightarrow a + b - 2c = 3, \\
\text{Yukawa terms} & \rightarrow a - c = 2n \text{ and } b - c = n.
\end{aligned} \tag{4}$$

Once we solve the above set of equations together, we have only two different choices for the $B-L$ charges,

$$(a, b, c, n) = (1, 0, -1, 1) \text{ and } \left(\frac{4}{3}, \frac{1}{3}, -\frac{2}{3}, 1 \right). \tag{5}$$

In the following, we choose the option for the fractional charges $\left(\frac{4}{3}, \frac{1}{3}, -\frac{2}{3}, 1 \right)$ to continue our phenomenology. If we consider the other choices with integer charges, we open up the Majorana mass terms for them and the Yukawa interaction terms with the lepton doublet, which will open up decay modes, thereby eliminating the DM candidate. This scenario is similar to the case for the $U(1)_{B-L}$ gauge symmetry with three right-handed neutrinos cancelling the gauge anomalies, which can decay into the SM sector very easily [15].

B. Scalar sector

In the present work, we have one scalar doublet and two singlet scalars, so we expand them, after the symmetry breaking, as follows,

$$\phi_h = \begin{pmatrix} G^+ \\ \frac{v+h+iG^0}{\sqrt{2}} \end{pmatrix}, \quad \phi_1 = \frac{v_1 + H_1 + iA_1}{\sqrt{2}}, \quad \phi_2 = \frac{v_2 + H_2 + iA_2}{\sqrt{2}}. \tag{6}$$

After the symmetry breaking, we consider the tadpole conditions with respect to h, H_1, H_2 , and take the values of other fields equal to zero, to get

$$\begin{aligned}\mu_h^2 &= \frac{1}{2} [2\lambda_h v_h^2 + \lambda_{h1} v_1^2 + \lambda_{h2} v_2^2], \\ \mu_1^2 &= \frac{1}{2} [2\lambda_1 v_1^2 + \lambda_{h1} v_h^2 + v_2 (2\sqrt{2}\mu + \lambda_{12} v_2)], \\ \mu_2^2 &= \frac{1}{2} \left[2\lambda_2 v_2^2 + \lambda_{h2} v_h^2 + \lambda_{12} v_1^2 + \frac{\sqrt{2}\mu v_1^2}{v_2} \right].\end{aligned}\quad (7)$$

From the second derivative of the scalar potential with respect to the fields and the tadpole conditions, we can have the neutral Higgs mass matrix in the basis $(h \ H_1 \ H_2)$,

$$M_{scalar}^2 = \begin{pmatrix} 2\lambda_h v_h^2 & \lambda_{h1} v_h v_1 & \lambda_{h2} v_h v_2 \\ \lambda_{h1} v_h v_1 & 2\lambda_1 v_1^2 & v_1 (\sqrt{2}\mu + \lambda_{12} v_2) \\ \lambda_{h2} v_h v_2 & v_1 (\sqrt{2}\mu + \lambda_{12} v_2) & \left(-\frac{\mu v_1^2}{\sqrt{2}v_2} + 2\lambda_2 v_2^2\right) \end{pmatrix}.\quad (8)$$

We can diagonalise the above neutral Higgs mass matrix by the unitary matrix and the mass eigenstates, $(h_1 \ h_2 \ h_3)$, can be introduced in the following way,

$$\begin{pmatrix} h \\ H_1 \\ H_2 \end{pmatrix} = U_{ij} \begin{pmatrix} h_1 \\ h_2 \\ h_3 \end{pmatrix}\quad (9)$$

where the unitary matrix U_{ij} ($i, j = 1, 2, 3$) can be expressed as

$$U_{ij} = \begin{pmatrix} c_{12}c_{13} & s_{12}c_{13} & s_{13} \\ -s_{12}c_{23} - c_{12}s_{23}s_{13} & c_{13}c_{23} - s_{12}s_{23}s_{13} & s_{23}c_{13} \\ s_{12}s_{23} - c_{12}c_{23}s_{13} & -c_{12}s_{23} - s_{12}c_{23}s_{13} & c_{23}c_{13} \end{pmatrix}.\quad (10)$$

In the same way, we can write down the mass matrix for the CP odd eigenstates in the basis $(A_1 \ A_2)$, as follows,

$$M_{CP-odd}^2 = \begin{pmatrix} -2\sqrt{2}\mu v_2 & \sqrt{2}\mu v_1 \\ \sqrt{2}\mu v_1 & -\frac{\mu v_1}{\sqrt{2}v_2} \end{pmatrix}.\quad (11)$$

There is also a Goldstone boson associated with the SM Z boson is independent of the other CP odd states. We can diagonalise the CP-odd mass matrix and get the eigenvalues as

$$M_A^2 = -2\sqrt{2}\mu v_2 \left(1 + \frac{v_1^2}{4v_2^2}\right), \quad M_{GBL} = 0.\quad (12)$$

Here, the mass eigenstates for the CP odd eigenstates are obtained in the following way,

$$\begin{pmatrix} G_{BL} \\ A \end{pmatrix} = \begin{pmatrix} \cos \beta & -\sin \beta \\ \sin \beta & \cos \beta \end{pmatrix} \begin{pmatrix} A_1 \\ A_2 \end{pmatrix} \quad (13)$$

where $\sin \beta = \frac{1}{\sqrt{1 + \frac{v_1^2}{4v_2^2}}}$, $\cos \beta = \frac{v_1}{2v_2\sqrt{1 + \frac{v_1^2}{4v_2^2}}}$ and $\tan \beta = \frac{2v_2}{v_1}$. In the above notation, G_{BL} is associated with the Goldstone boson for the $U(1)_{B-L}$ gauge boson whose mass is given by

$$\begin{aligned} M_{Z_{BL}}^2 &= g_{BL}^2 v_1^2 + 4g_{BL}^2 v_2^2 \\ &= g_{BL}^2 v_1^2 (1 + \tan^2 \beta) \end{aligned} \quad (14)$$

C. Singlet fermion masses and interactions

Once the singlet scalars take the VEVs, we can write down the mass term for the BSM fermions as follows,

$$\mathcal{L}_{\xi\chi} = \begin{pmatrix} \bar{\xi}_{1L} & \bar{\xi}_{2L} \end{pmatrix} \begin{pmatrix} \frac{\alpha_1 v_2}{\sqrt{2}} & \frac{\beta_2 v_2}{\sqrt{2}} \\ \frac{\beta_1 v_1}{\sqrt{2}} & \frac{\alpha_2 v_1}{\sqrt{2}} \end{pmatrix} \begin{pmatrix} \chi_{1R} \\ \chi_{2R} \end{pmatrix} + h.c. \quad (15)$$

We can relate the singlet fermions to the left-handed and right-handed fermions of two Dirac mass eigenstates, $\psi_{1,2} = \psi_{1,2L} \oplus \psi_{1,2R}$, by

$$\begin{pmatrix} \xi_{1L} \\ \xi_{2L} \end{pmatrix} = U_L \begin{pmatrix} \psi_{1L} \\ \psi_{2L} \end{pmatrix}, \quad \begin{pmatrix} \chi_{1R} \\ \chi_{2R} \end{pmatrix} = U_R \begin{pmatrix} \psi_{1R} \\ \psi_{2R} \end{pmatrix}, \quad \text{with } U_{L,R} = \begin{pmatrix} \cos \theta_{L,R} & \sin \theta_{L,R} \\ -\sin \theta_{L,R} & \cos \theta_{L,R} \end{pmatrix}. \quad (16)$$

Therefore, using the above field redefinitions, we can write down

$$\begin{pmatrix} M_1 & 0 \\ 0 & M_2 \end{pmatrix} = U_L^T \begin{pmatrix} \frac{\alpha_1 v_2}{\sqrt{2}} & \frac{\beta_2 v_2}{\sqrt{2}} \\ \frac{\beta_1 v_1}{\sqrt{2}} & \frac{\alpha_2 v_1}{\sqrt{2}} \end{pmatrix} U_R \quad (17)$$

where $M_{1,2}$ are the masses of the Dirac fermions. The fermionic mixing angles $\theta_{L,R}$ can be represented such that $\theta_{L,R} \rightarrow 0$ as $\beta_{1,2} \rightarrow 0$, and the limits are still true for $\alpha_2 \ll 1$. The fermionic mixing angles, $\theta_{L,R}$, can be written in terms of the Yukawa couplings, $\alpha_{1,2}$ and $\beta_{1,2}$, and physical fermion masses, $M_{1,2}$, in the following way,

$$\begin{aligned} \tan \theta_R &= \frac{M_1 v_2 \beta_2 + M_2 v_1 \beta_1}{M_2 v_1 \alpha_2 - M_1 v_2 \alpha_1}, \\ \tan \theta_L &= \frac{M_1 \alpha_1 \tan \theta_R + \beta_1}{M_2 \alpha_1 - \beta_2 \tan \theta_R}. \end{aligned} \quad (18)$$

We see from the above relation that if we fix the θ_R then θ_L is automatically fixed with different values. Finally, the Yukawa terms associated with the BSM fermions $\psi_{1,2}$ and the Higgs bosons, $h_{1,2,3}$, take the following form,

$$\begin{aligned}
\mathcal{L}_\psi^{Yuk} &= \sum_{i=1,2,3} \alpha_{11i} \bar{\psi}_{1L} \psi_{1R} h_i + \sum_{i=1,2,3} \alpha_{12i} \bar{\psi}_{1L} \psi_{2R} h_i + \sum_{i=1,2,3} \alpha_{21i} \bar{\psi}_{2L} \psi_{1R} h_i \\
&+ \sum_{i=1,2,3} \alpha_{22i} \bar{\psi}_{2L} \psi_{2R} h_i + i \alpha_{11A} \bar{\psi}_{1L} \psi_{1R} A + i \alpha_{12A} \bar{\psi}_{1L} \psi_{2R} A + i \alpha_{21A} \bar{\psi}_{2L} \psi_{1R} A \\
&+ i \alpha_{22A} \bar{\psi}_{2L} \psi_{2R} A + h.c..
\end{aligned} \tag{19}$$

where the Yukawa interactions for physical states take the following form,

$$\begin{aligned}
\alpha_{11i} &= \frac{M_1}{\sqrt{2}v_1v_2} [U_{3i}v_1 + U_{2i}v_2 + (U_{3i}v_1 - U_{2i}v_2) \cos 2\theta_L] , \\
\alpha_{12i} &= \frac{\sqrt{2}M_2}{v_1v_2} [(U_{3i}v_1 - U_{2i}v_2) \cos \theta_L \sin \theta_L] , \\
\alpha_{21i} &= \frac{\sqrt{2}M_1}{v_1v_2} [(U_{3i}v_1 - U_{2i}v_2) \cos \theta_L \sin \theta_L] , \\
\alpha_{22i} &= \frac{M_2}{\sqrt{2}v_1v_2} [U_{3i}v_1 + U_{2i}v_2 + (-U_{3i}v_1 + U_{2i}v_2) \cos 2\theta_L] .
\end{aligned} \tag{20}$$

Here, the matrix U is defined in Eq. (10), and $U_{3A} = \cos \beta$ and $U_{2A} = \sin \beta$ for $i = A$.

In the basis of the mass eigenstates $\psi_{1,2}$, we can have the $U(1)_{B-L}$ gauge interaction terms with the gauge boson Z_{BL} , as follows,

$$\begin{aligned}
\mathcal{L}_{\psi Z_{BL}} &= -\frac{g_{BL}}{3} \left[\bar{\psi}_1 \gamma^\mu ((3 \cos^2 \theta_L + 1)P_L - 2P_R) \psi_1 + \bar{\psi}_2 \gamma^\mu ((3 \sin^2 \theta_L + 1)P_L - 2P_R) \psi_2 \right. \\
&\left. + \bar{\psi}_1 \gamma^\mu (2 \sin^2 \theta_L) P_L \psi_2 + \bar{\psi}_2 \gamma^\mu (2 \sin^2 \theta_L) P_L \psi_1 \right] Z_{BL\mu} .
\end{aligned} \tag{21}$$

For the later discussion, we consider ψ_1 as WIMP-type DM and ψ_2 as FIMP DM, with the associated couplings in the freeze-out and freeze-in regimes, respectively. This can be achieved easily when $v_1 \gg v_2$ and all the BSM particle masses are in the sub-TeV range. Then, we can see that the extra gauge coupling g_{BL} and the Yukawa couplings α_{22i} fall in the feeble regime whereas the Yukawa couplings α_{11i} are in the freeze-out regime. If $\theta_L = 0$, a stable two-component dark matter composed of WIMP and FIMP is possible. Otherwise, the heavier one will decay into the lighter one, leaving only one component DM.

D. Neutrino masses

For the particle content with the $U(1)_{B-L}$ gauge symmetry, the neutrino masses can be generated by introducing an additional triplet scalar, as has been studied in Ref. [21] or by introducing

the right-handed neutrinos through inverse seesaw mechanism Ref. [22]. In our model, we anticipate higher-dimensional operators for Majorana neutrino masses that are $U(1)_{B-L}$ gauge invariant,

$$\mathcal{L}_{Neutrino} = \kappa_{ij} \frac{(L_i \phi_h)(L_j \phi_h)}{\Lambda} \frac{\phi_1^2}{\Lambda^2} + \kappa'_{ij} \frac{(L_i \phi_h)(L_j \phi_h)}{\Lambda} \frac{\phi_2}{\Lambda} + h.c.. \quad (22)$$

where $\kappa_{ij}, \kappa'_{ij}$ ($i, j = 1, 2, 3$) are the coefficients and Λ is the cut-off scale. The higher-dimensional terms can be originated from the extension of the current set-up with three additional right-handed fermions that are singlets under the SM gauge group but charged under the $U(1)_{B-L}$ in such a way that the gauge anomalies remain cancelled. With these additional fermions, we can realize the Type-I seesaw mechanism for the generation of light active neutrino masses. In Table III, we show the $U(1)_{B-L}$ charge assignment for the additional right-handed singlets which does not affect the gauge anomaly condition.

Gauge Group	Fermionic Fields		
	N_1	N_2	N_3
$SU(2)_L$	1	1	1
$U(1)_{B-L}$	1	-1	0

Table III: Right-handed singlet fermions and their corresponding charges under $SU(2)_L$ and $U(1)_{B-L}$ gauge groups. All the additional fermions have zero hypercharges.

The Lagrangian for the additional right-handed fermions up to dimension-5 operators, which are allowed under SM and $U(1)_{B-L}$ gauge groups, can be written as

$$\begin{aligned} \mathcal{L}_N = & y_{e1} \bar{L}_e \tilde{\phi}_h N_1 \frac{\phi_2}{\Lambda} + y_{e2} \bar{L}_e \tilde{\phi}_h N_2 + y_{e3} \bar{L}_e \tilde{\phi}_h N_3 \frac{\phi_1}{\Lambda} + y_{\mu 1} \bar{L}_\mu \tilde{\phi}_h N_1 \frac{\phi_2}{\Lambda} + y_{\mu 2} \bar{L}_\mu \tilde{\phi}_h N_2 \\ & + y_{\mu 3} \bar{L}_\mu \tilde{\phi}_h N_3 \frac{\phi_1}{\Lambda} + y_{\tau 1} \bar{L}_\tau \tilde{\phi}_h N_1 \frac{\phi_2}{\Lambda} + y_{\tau 2} \bar{L}_\tau \tilde{\phi}_h N_2 + y_{\tau 3} \bar{L}_\tau \tilde{\phi}_h N_3 \frac{\phi_1}{\Lambda} + Y_{11} N_1 N_1 \phi_2 \\ & + Y_{12} N_1 N_2 \phi_2 + Y_{13} N_1 N_3 \phi_2 + Y_{22} N_2 N_2 \phi_2 + Y_{23} N_2 N_3 \phi_1 + M_{33} N_3 N_3 + h.c.. \end{aligned} \quad (23)$$

Once the $U(1)_{B-L}$ symmetry is spontaneously broken, we can write the neutrino mass matrix in the $(\nu_{L,i}^c \ N_i)^T$ basis, as follows,

$$\mathcal{L}_{N-mass} = \begin{pmatrix} \bar{\nu}_{L,i}^c & \bar{N}_i \end{pmatrix} \begin{pmatrix} 0 & m_D \\ m_D^T & M_R \end{pmatrix} \begin{pmatrix} \nu_{L,i}^c \\ N_i^c \end{pmatrix} + h.c. \quad (24)$$

where the Dirac (m_D) and Majorana (M_R) mass matrices are,

$$m_D = \begin{pmatrix} \frac{y_{e1}vv_2}{2\Lambda} & \frac{y_{e2}v}{\sqrt{2}} & \frac{y_{e3}vv_1}{2\Lambda} \\ \frac{y_{\mu 1}vv_2}{2\Lambda} & \frac{y_{\mu 2}v}{\sqrt{2}} & \frac{y_{\mu 3}vv_1}{2\Lambda} \\ \frac{y_{\tau 1}vv_2}{2\Lambda} & \frac{y_{\tau 2}v}{\sqrt{2}} & \frac{y_{\tau 3}vv_1}{2\Lambda} \end{pmatrix}, \quad M_R = \begin{pmatrix} \frac{Y_{11}v_2}{\sqrt{2}} & \frac{Y_{12}v_2}{\sqrt{2}} & \frac{Y_{13}v_1}{\sqrt{2}} \\ \frac{Y_{12}v_2}{\sqrt{2}} & \frac{Y_{22}v_2}{\sqrt{2}} & \frac{Y_{23}v_1}{\sqrt{2}} \\ \frac{Y_{13}v_1}{\sqrt{2}} & \frac{Y_{23}v_1}{\sqrt{2}} & M_{33} \end{pmatrix}. \quad (25)$$

Once we diagonalize the above neutrino mass matrix in the limit with $M_R \gg m_D$, we can write down the light neutrino mass matrix (m_ν) and the heavy neutrino mass matrix (M_N) as,

$$m_\nu \simeq -m_D^T M_R^{-1} m_D, \quad M_N \simeq M_R \quad (26)$$

Then, we can use the above mass matrices to get the neutrino masses and the correct oscillation parameters easily [28]. For example, if we consider the masses of the right-handed fermions to be $M_{N,ij} \sim \text{TeV}$, we only have to take the Dirac mass masses to be $m_{D,ij} \sim 10^{-4} \text{ GeV}$ to obtain the light neutrino masses of order 0.01 eV. There are free parameters in M_R and m_D , y_{fi} and Y_{ij} ($f = e, \mu, \tau$ and $i, j = 1, 2, 3$) and Λ , which give us the freedom to make each component fall within the suitable range, even if v_1 and v_2 are hierarchical. Moreover, if we demand that the cut-off scale is higher than $v_{1,2}$ and $v_1 \gg v_2$, then $m_{D,11}, m_{D,21}, m_{D,31}$ become subdominant, but we still have enough free parameters to account for the neutrino oscillation parameters.

III. CONSTRAINTS

In this section, we discuss various constraints on the model, such as perturbativity bounds, vacuum stability bounds for theoretical consistency, and experimental bounds such as DM relic density, DM direct and indirect detection bounds, collider bounds (mainly from Higgs decays), bounds from BBN and oblique parameters.

A. Perturbativity bounds

The quartic couplings in the scalar potential can be written in terms of the masses and the mixing angles for the scalar fields, as follows,

$$\begin{aligned}
\lambda_h &= \frac{U_{11}^2 M_{h_1}^2 + U_{12}^2 M_{h_2}^2 + U_{13}^2 M_{h_3}^2}{2v_h^2}, \\
\lambda_1 &= \frac{U_{21}^2 M_{h_1}^2 + U_{22}^2 M_{h_2}^2 + U_{23}^2 M_{h_3}^2}{2v_1^2}, \\
\lambda_2 &= \frac{U_{31}^2 M_{h_1}^2 + U_{32}^2 M_{h_2}^2 + U_{33}^2 M_{h_3}^2 - M_A^2 \cos^2 \beta}{2v_2^2}, \\
\lambda_{h_1} &= \frac{U_{11}U_{21}M_{h_1}^2 + U_{12}U_{22}M_{h_2}^2 + U_{13}U_{23}M_{h_3}^2}{v_h v_1}, \\
\lambda_{h_2} &= \frac{U_{11}U_{31}M_{h_1}^2 + U_{12}U_{32}M_{h_2}^2 + U_{13}U_{33}M_{h_3}^2}{v_h v_2}, \\
\lambda_{12} &= \frac{U_{21}U_{31}M_{h_1}^2 + U_{22}U_{32}M_{h_2}^2 + U_{23}U_{33}M_{h_3}^2 + M_A^2 \sin \beta \cos \beta}{v_1 v_2}.
\end{aligned} \tag{27}$$

In the following analysis, we assume that all the quartic couplings are in the perturbative regime, namely, between 0 and 4π .

B. Vacuum stability bounds

The bound from the below of the potential for the higher values of the fields can be expressed in terms of the quartic couplings in the following way,

$$\begin{aligned}
\lambda_h > 0, \lambda_1 > 0, \lambda_2 > 0, \lambda_{12} + 2\sqrt{\lambda_1 \lambda_2} > 0, -2\sqrt{\lambda_h \lambda_1} \leq \lambda_{h_1} \leq 2\sqrt{\lambda_h \lambda_1}, \\
-2\sqrt{\lambda_h \lambda_2} \leq \lambda_{h_2} \leq 2\sqrt{\lambda_h \lambda_2}, 2\lambda_h \lambda_{12} - \lambda_{h_1} \lambda_{h_2} + \sqrt{(4\lambda_h \lambda_1 - \lambda_{h_1}^2)(4\lambda_h \lambda_2 - \lambda_{h_2}^2)} \geq 0.
\end{aligned} \tag{28}$$

C. DM relic density

In our model, we can account for the Planck constraints on the total DM relic density, incorporating the contributions from both the WIMP and FIMP DM components. Specifically, we consider a 7σ variation in the DM relic density obtained from Planck 2018 [29], as detailed below,

$$0.1116 \leq (\Omega_{\psi_1} + \Omega_{\psi_2}) h^2 \leq 0.1284. \tag{29}$$

D. DM direct detection bounds

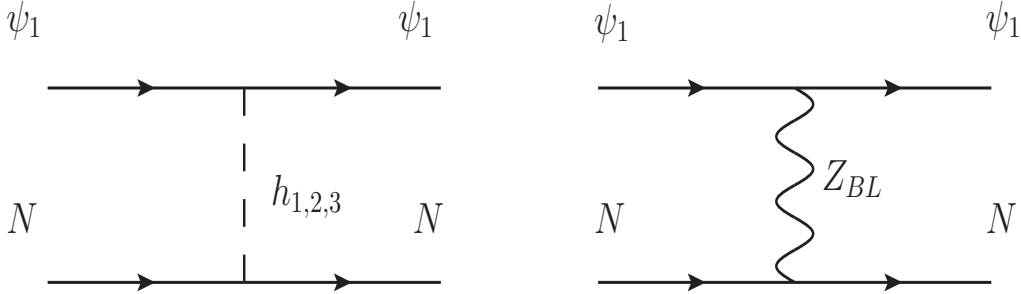


Figure 1: Direct detection processes relevant in our study.

The direct detection cross-section for the DM-nucleus scattering process, $\psi_1 N \rightarrow \psi_1 N$ (as shown in Fig. 1) can be expressed in the non-relativistic limit, as follows,

$$\sigma_{\psi_1} = \frac{\mu^2}{\pi} \left[\frac{f_N M_N}{v} \sum_{i=1,2,3} \frac{U_{1i} \alpha_{11i}}{M_{h_i}^2} + \frac{f_{Z_{BL}} g_{BL}^2 (3 \cos^2 \theta_L - 1)}{18 M_{Z_{BL}}^2} \right]^2 \quad (30)$$

where $\mu = \frac{M_{\psi_1} M_N}{M_{\psi_1} + M_N}$ and $f_N \sim 0.3$ [30], $f_{Z_{BL}} = 3$ [31]. In our study, we consider the multi-component DM scenario, so we need to multiply by the fraction of ψ_1 DM component, f_{ψ_1} , for the DD direction bounds, when compared with the recent LUX-ZEPLIN data [1].

E. DM indirect detection bounds

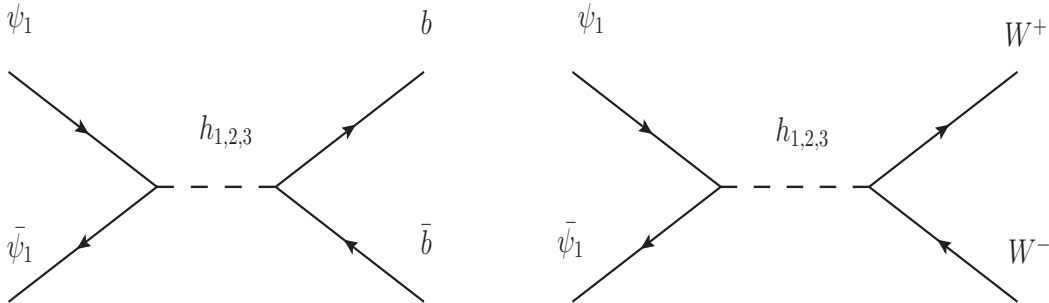


Figure 2: Indirect detection processes relevant in our study.

The WIMP DM in our study can also be detected at the indirect detection (ID) experiments when DM annihilates into the SM particles. There are many experiments deployed for this purpose like Fermi-LAT [32] and many planned experiments are underway like Cherenkov Telescope

Array [33]. The indirect detection estimates when DM annihilation into the SM final states can be summarised as follows,

$$\begin{aligned}
(\sigma v)_{kk} &\simeq \frac{n_c v_{rel}^2 M_b^2 M_{\psi_1}^2 \left(1 - \frac{M_b^2}{M_{\psi_1}^2}\right)^{3/2}}{8\pi v^2} \sum_{i,j=1,2,3} A_i A_j^*, \text{ for } k = b, \\
&\simeq \frac{v_{rel}^2 M_W^4 \sqrt{1 - \frac{M_W^2}{M_{\psi_1}^2}}}{16\pi v^2} \left(3 - \frac{4M_{\psi_1}^2}{M_W^2} + \frac{4M_{\psi_1}^4}{M_W^4}\right) \sum_{i,j=1,2,3} A_i A_j^*, \text{ for } k = W^\pm. \quad (31)
\end{aligned}$$

where $n_c = 3$ is colour charge, $v_{rel} \sim 10^{-3}$ is the DM velocity in the present time and A_i can be expressed as,

$$A_i = \frac{\alpha_{11i} U_{1i}}{(4M_{\psi_1}^2 - M_{h_i}^2) + i\Gamma_{h_i} M_{h_i}}. \quad (32)$$

Our WIMP DM is fermionic, so we always have p-wave annihilation to the SM final state particles which is suppressed by the square of the DM velocity in the present time. Therefore, our WIMP DM is hard to detect at the present time by the indirect detection experiments and possible to explore in future with increased sensitivity like the Cherenkov Telescope Array [33].

F. Collider bounds

We have not performed a dedicated study of the present model for colliders but we can constrain our model with the other well known searches for the SM. The precise measurements of the SM Higgs observables, like the Higgs signal strength and Higgs invisible decay can put severe bounds on the BSM scenarios for any deviation from DM. So, we briefly discuss them below and take a small Higgs mixing angle to accommodate the Higgs bounds in our work.

Higgs signal strengths: The SM Higgs boson has been measured very precisely so any deviation from the standard scenario will be tightly constrained. Bound from the Higgs signal strength measurement is one such measurement. We assume that Higgs produces on-shell and then it decays to some SM final states. In these assumptions, we can factorise the SM Higgs signal strength in two parts, one is associated with production and the second one is associated with its decay branching. Therefore, we can write down the SM Higgs signal strength as,

$$\begin{aligned}
\mu &= \mu_h^{Prod} \mu_h^{Br} \\
&= \frac{\sigma_{h_1}^{Prod}}{\sigma_{H_{SM}}^{Prod}} \times \frac{Br_h}{Br_{H_{SM}}}. \quad (33)
\end{aligned}$$

In our case, the Higgs production with the SM Higgs boson will be proportional to the cosine of the neutral Higgs mixing angle *i.e.* $\mu_h^{Prod} = \cos^2 \theta_{12} \cos^2 \theta_{13}$. On the other ratio of the branchings can be expressed as,

$$\begin{aligned} \mu_h^{Br} &= \frac{Br_h}{Br_{H_{SM}}} \\ &= \frac{\Gamma_{h_1 \rightarrow SM}}{\Gamma_{H_{SM} \rightarrow SM}} \times \frac{\Gamma_{h_1}^{tot}}{\Gamma_{h_1}^{tot} + \Delta\Gamma_{h_1}} \end{aligned} \quad (34)$$

where $\Delta\Gamma_{h_1}$ is the extra decay mode which SM like Higgs may have due to the additional particles. In our work, SM like Higgs has similar branching with the SM Higgs, so the ratio we take is 1 in our work. In Ref. [34], authors have considered LHC run 2 data from ATLAS [35] and CMS [36] detectors along with the less significant LHC run 1 [37] and Tevatron data [38] and combinedly found the SM Higgs signal strength at the 1σ range as,

$$\mu^{Combine} = 1.012 \pm 0.034. \quad (35)$$

Therefore, at 2σ range we need to satisfy $\cos^2 \theta_{12} \cos^2 \theta_{13} \geq 0.944$ and assuming θ_{13} small, we get $\sin \theta_{12} \leq 0.23$.

Higgs invisible decays: We have the DM components which can be produced from the Higgs decays at the colliders if their masses are smaller than the half of the SM Higgs boson mass. The presence of the SM Higgs boson decays can be inferred from the large missing momentum along the direction of the Higgs boson momentum. Dedicated searches for such invisible modes of the SM Higgs has put bounds on the Higgs invisible branching ratio (Br_{inv}) by $Br_{inv} < 0.16$ at 95% confidence level [39–41].

The bounds associated with the additional gauge boson Z_{BL} from colliders, mainly LEP and LHC [42–45], are unimportant in our study, because we have considered the feeble regime of the additional gauge coupling.

G. BBN bounds

As discussed before and will be discussed in detail later, the gauge coupling g_{BL} , we have considered in the feeble regime, therefore, the additional $U(1)_{B-L}$ gauge boson, Z_{BL} , has the possibility to decay after BBN which is roughly 1 sec. This decay will hamper the successful prediction of BBN by injecting more electromagnetic energy [46] and hinder the nucleation process. We have estimated that for a most liberal case $M_{Z_{BL}} = 1$ GeV, we need $g_{BL} > 2 \times 10^{-12}$ for making Z_{BL} decays before BBN and as we increase the Z_{BL} mass the limit gets lower. In the concourse of our study, we have taken care of the BBN bound.

H. Oblique parameters

The oblique parameters, S, T and U , can be obtained from Ref. [47], as

$$\begin{aligned}
S &= \frac{1}{24\pi} \left[U_{11}^2 \ln M_{h_1}^2 + U_{12}^2 \ln M_{h_2}^2 + U_{13}^2 \ln M_{h_3}^2 - \ln M_{h_{SM}}^2 + U_{11}^2 \hat{G}(M_{h_1}^2, M_Z^2) \right. \\
&\quad \left. + U_{12}^2 \hat{G}(M_{h_2}^2, M_Z^2) + U_{13}^2 \hat{G}(M_{h_3}^2, M_Z^2) - \hat{G}(M_{h_{SM}}^2, M_Z^2) \right], \\
T &= \frac{1}{16\pi^2 M_W^2 s_w^2} \left[3U_{11}^2 \left(F(M_Z^2, M_{h_1}^2) - F(M_W^2, M_{h_1}^2) \right) + 3U_{12}^2 \left(F(M_Z^2, M_{h_2}^2) - F(M_W^2, M_{h_2}^2) \right) \right. \\
&\quad \left. + 3U_{13}^2 \left(F(M_Z^2, M_{h_3}^2) - F(M_W^2, M_{h_3}^2) \right) - 3 \left(F(M_Z^2, M_{h_{SM}}^2) - F(M_W^2, M_{h_{SM}}^2) \right) \right], \\
U &= \frac{1}{24\pi} \left[U_{11}^2 \left(\hat{G}(M_{h_1}^2, M_W^2) - \hat{G}(M_{h_1}^2, M_Z^2) \right) + U_{12}^2 \left(\hat{G}(M_{h_2}^2, M_W^2) - \hat{G}(M_{h_2}^2, M_Z^2) \right) \right. \\
&\quad \left. + U_{13}^2 \left(\hat{G}(M_{h_3}^2, M_W^2) - \hat{G}(M_{h_3}^2, M_Z^2) \right) - \left(\hat{G}(M_{h_{SM}}^2, M_W^2) - \hat{G}(M_{h_{SM}}^2, M_Z^2) \right) \right], \quad (36)
\end{aligned}$$

where U_{ij} ($i, j = 1, 2, 2$) is the Higgses mixing matrix defined in Eq. (10). As we will see since we have considered small mixing angles among the scalars, demanded from the Higgs collider searches, so there are small contributions to the oblique parameters, which are safe from the current bounds on S, T, U [48–51].

IV. RESULTS

In this section, we present the main results for the parameter space in the model by considering various constraints discussed in the previous section and identify the survived region in terms of physical masses and couplings for the extra particles as well as the predicted values for the DD and ID detection cross sections.

A. Constraints

Taking into account the perturbativity bounds and the vacuum stability conditions, we consider the following ranges of the model parameters,

$$\begin{aligned}
10^{-4} &\leq \theta_{12} \leq 0.23, \quad 10^{-4} \leq \theta_{13,23} \leq 0.1, \quad 10^{-12} \leq g_{BL} \leq 10^{-8}, \quad \theta_{L,R} = 0, \\
1 &\leq (M_{h_{2,3}} - M_{h_1}) [\text{GeV}] \leq 10^3, \quad 1 \leq (M_A - M_{h_1}) [\text{GeV}] \leq 10^3, \\
1 &\leq M_{Z_{BL}} [\text{GeV}] \leq 10^3, \quad 10^{-12} \leq \tan \beta \leq 10^{-8}. \quad (37)
\end{aligned}$$

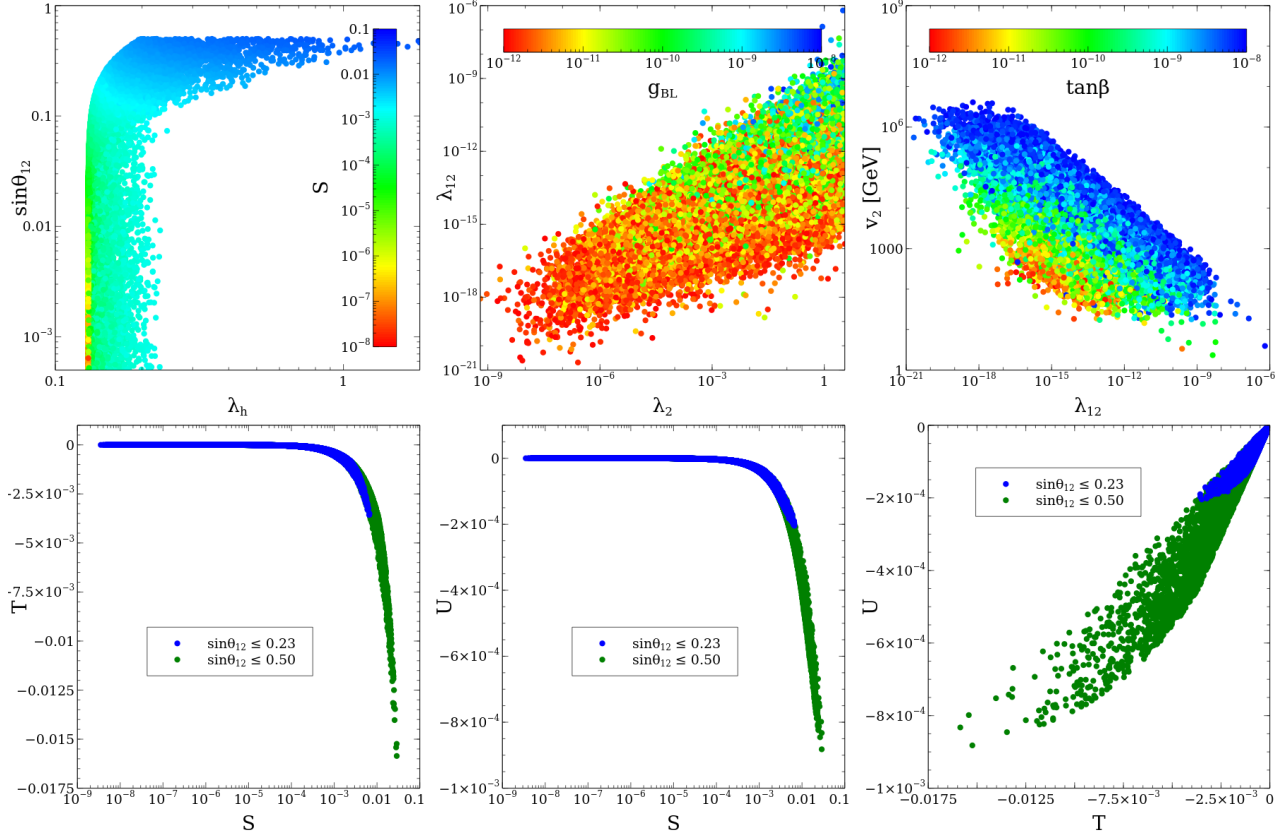


Figure 3: Variation in different parameter spaces consists of quartic couplings, mixing angle and oblique parameters. The points have been obtained after satisfying the perturbativity and potential bound from the below constraints.

In Fig. 3, we have shown the scattered plots among the different parameter spaces after varying the model parameters in the range shown in Eq. (37). In the top panel, we have shown the allowed region in the $\lambda_h - \sin\theta_{12}$, $\lambda_2 - \lambda_{12}$, and $\lambda_{12} - v_2$ planes after incorporating the perturbativity and vacuum stability bounds. In the top left panel, we can see that for $\sin\theta_{12} < 0.1$, the value of λ_h is independent of the increment in $\sin\theta_{12}$, and once $\sin\theta_{12}$ goes beyond 0.1, λ_h starts increasing. This is because, for larger values of the mixing angle, the contribution from the BSM Higgses becomes effective. The colour bar represents the different values of the oblique parameter S , and it never goes beyond 0.1 for the chosen parameter range. In the top middle panel, we have shown the plot in the $\lambda_2 - \lambda_{12}$ plane, and the colour bar shows the different values of g_{BL} . We can see a correlation between the quartic couplings, and this is the effect of the v_2 VEV because both of them depend on the VEV v_2 . From the colour bar, we can see that as the gauge coupling values increase, we observe an increase in the λ_{12} values, which implies that the VEV v_1 decreases. However, there is no straightforward relation for λ_2

because the VEV v_2 is subdominant compared to v_1 in our study. In the top right panel, we have shown the scatter plot in the $\lambda_{12} - v_2$ plane, where the colour bar shows the different values of $\tan \beta$. From the figure, we can see an anti-correlation between them, which is expected because λ_{12} is inversely proportional to v_2 . Moreover, $\tan \beta$ is linearly proportional to the VEV v_2 , which can be easily seen from the colour bar.

In the lower panel of Fig. 3, we have shown the scatter plot among the oblique parameters S , T , and U . All the values are allowed by the existing bounds on the oblique parameters [48–51], and we do not have significant deviations from the Standard Model (SM). We also observe a nice correlation among them, although they are small for most of the allowed regions. The smallness of S , T , and U is mainly due to the smaller values of the mixing angles θ_{12} , θ_{23} , and θ_{13} which ensures the safety from the collider bound. We have shown the blue and red points for different upper limits of $\sin \theta_{12}$, and the allowed ranges are larger when we choose a larger upper limit on $\sin \theta_{12}$.

B. DM results

In the present work, we explore the alternate scenario in the context of $U(1)_{B-L}$ model where we have taken additional fermions instead of the usual right handed neutrinos [16–20] for the cancellation of gauge anomalies. We focus on the WIMP and FIMP combination of DM, demanding the extra gauge coupling to be in the feeble regime. The feeble coupling also makes the additional gauge boson Z_{BL} out of equilibrium and hence we need to consider the non-thermal nature of the distribution of Z_{BL} for a treatment of the Z_{BL} decay. However, we show later that it is sufficient to take the Maxwell-Boltzmann distribution for Z_{BL} in order to obtain the result from the Z_{BL} decay.

The distribution function for the Z_{BL} can be determined from the following Boltzmann equation,

$$\hat{L}f_{Z_{BL}} = \sum_{i=1,2,3} \mathcal{C}^{h_i \rightarrow Z_{BL}Z_{BL}} + \sum_{B,C=A,h_i} \mathcal{C}^{B \rightarrow Z_{BL}C} + \mathcal{C}^{Z_{BL} \rightarrow All} \quad (38)$$

where the Liouville's operator, \hat{L} , can be expressed as,

$$\hat{L} = zH \left(1 + \frac{Tg'_s}{3g_s} \right) \frac{\partial}{\partial z}. \quad (39)$$

In the above equation, the left-hand side corresponds to the DM evolution due to the expansion of the Universe and the right-hand side implies the collision functions associated with the additional gauge boson Z_{BL} . The form of the collision functions, $\mathcal{C}^{h_i \rightarrow Z_{BL}Z_{BL}}$, $\mathcal{C}^{B \rightarrow Z_{BL}C}$ and $\mathcal{C}^{Z_{BL} \rightarrow All}$, have been shown in the Appendix.

The Boltzmann equations for the DM candidates, ψ_1 and ψ_2 , and the next to stable particle Z_{BL} , can be expressed as

$$\begin{aligned}
\frac{dY_{\psi_1}}{dz} &= -\frac{S(z_{\psi_1})\langle\sigma v\rangle_{\psi_1\psi_1}}{z_{\psi_1}H(z_{\psi_1})}\left(Y_{\psi_1}^2 - Y_{\psi_1}^{eq2}\right) \\
&\quad - \sum_{A=h_i, Z_{BL}} \theta(M_{\psi_1} - M_{\psi_2} - M_A) \frac{M_{pl}z\sqrt{g_{eff}}}{0.33M_{sc}^2g_{*,s}(z)} \left(\langle\Gamma_{\psi_1\rightarrow\psi_2A}\rangle (Y_{\psi_1}^{eq} - Y_{\psi_2}Y_A)\right), \\
\frac{dY_{Z_{BL}}}{dz} &= \sum_{B=h_i} \theta(M_B - 2M_{Z_{BL}}) \frac{2M_{pl}z\sqrt{g_{eff}}}{0.33M_{sc}^2g_{*,s}(z)} \langle\Gamma_{B\rightarrow Z_{BL}Z_{BL}}\rangle \left(Y_B^{eq} - Y_{Z_{BL}}^2\right) \\
&\quad + \sum_{B,C=h_i, A, \psi_1} \theta(M_B - M_C - M_{Z_{BL}}) \frac{M_{pl}z\sqrt{g_{eff}}}{0.33M_{sc}^2g_{*,s}(z)} \left(\langle\Gamma_{B\rightarrow CZ_{BL}}\rangle (Y_B^{eq} - Y_C Y_{Z_{BL}})\right) \\
&\quad - \sum_{C=All} \theta(M_{Z_{BL}} - 2M_C) \frac{M_{pl}z\sqrt{g_{eff}}}{0.33M_{sc}^2g_{*,s}(z)} \langle\Gamma_{Z_{BL}\rightarrow CC}\rangle_{NTH} \left(Y_{Z_{BL}} - Y_C^2\right) \Big], \\
\frac{dY_{\psi_2}}{dz} &= \sum_{B=h_i} \theta(M_B - 2M_{\psi_2}) \frac{2M_{pl}z\sqrt{g_{eff}}}{0.33M_{sc}^2g_{*,s}(z)} \langle\Gamma_{B\rightarrow\psi_2\psi_2}\rangle \left(Y_B^{eq} - Y_{\psi_2}^2\right) \\
&\quad + \theta(M_{Z_{BL}} - 2M_{\psi_2}) \frac{2M_{pl}z\sqrt{g_{eff}}}{0.33M_{sc}^2g_{*,s}(z)} \langle\Gamma_{Z_{BL}\rightarrow\psi_2\psi_2}\rangle_{NTH} \left(Y_{Z_{BL}} - Y_{\psi_2}^2\right) \\
&\quad + \sum_{A=h_i, Z_{BL}} \theta(M_{\psi_1} - M_{\psi_2} - M_A) \frac{M_{pl}z\sqrt{g_{eff}}}{0.33M_{sc}^2g_{*,s}(z)} \left(\langle\Gamma_{\psi_1\rightarrow\psi_2A}\rangle (Y_{\psi_1}^{eq} - Y_{\psi_2}Y_A)\right) \quad (40)
\end{aligned}$$

where

$$\langle\Gamma_{X\rightarrow BC}\rangle = \Gamma_{X\rightarrow BC} \frac{K_1(z_X)}{K_2(z_X)}, \quad \langle\Gamma_{Z_{BL}\rightarrow BC}\rangle_{NTH} = M_{Z_{BL}} \Gamma_{Z_{BL}\rightarrow BC} \frac{\int \frac{f_{Z_{BL}} d^3p}{\sqrt{p^2 + M_{Z_{BL}}^2}}}{\int f_{Z_{BL}} d^3p}. \quad (41)$$

In the above Boltzmann equations, we have used MicrOMEGAs [52] for solving the Boltzmann equation for the WIMP DM ψ_1 . To use MicrOMEGAs, we have implemented our model in FeynRules [53] and generated the CalcHEP [54] model files for the DM study. The co-moving number densities of FIMP DM ψ_2 and the next to stable particle Z_{BL} have been computed based on our own code. We have used the decay processes only in the estimation of FIMP components and ignored the annihilation contributions which are subdominant. contribution. We have modified the MicrOMEGAs code to implement the external codes for FIMP DM and generated the plots. Once we have the co-moving number densities for $\psi_{1,2}, Z_{BL}$ ($Y_{\psi_{1,2}}, Y_{Z_{BL}}$), we can determine their relic densities by using the following expression [55],

$$\Omega_P h^2 = 2.755 \times 10^8 \times Y_P \times \left(\frac{M_P}{\text{GeV}}\right) \quad \text{where } P = \psi_1, \psi_2, Z_{BL}. \quad (42)$$

In the next paragraph, we provide the analytical estimation of the FIMP DM components which matches pretty well with the output of the Boltzmann equations with maximum 10% deviation.

Analytical estimates: The FIMP DM production from the decays can be estimated by following Ref. [3]. If we consider a process $X \rightarrow P_{DM}Q$, then the relic density for FIMP DM we can estimate as follows,

$$\Omega_{P_{DM}} h^2 \simeq \frac{1.09 \times 10^{27} M_{P_{DM}} \Gamma_X}{g_\rho^{3/2} M_X^2} \quad (43)$$

where g_ρ is the relativistic matter *d.o.f* of the Universe during the production of DM, which is around $g_\rho \sim 100$ in our study. Therefore, we can estimate the production of Z_{BL} from the decays of the scalars and the ψ_2 production from the decays of the scalars and the extra gauge boson as follows,

$$\begin{aligned} \Omega_{Z_{BL}} h^2 &\simeq \sum_{X=h_{1,2,3}} \frac{2.18 \times 10^{27} M_{Z_{BL}} \Gamma_{X \rightarrow Z_{BL} Z_{BL}}}{g_\rho^{3/2} M_X^2} + \sum_{X,Q=h_{1,2,3,A}} \frac{1.09 \times 10^{27} M_{Z_{BL}} \Gamma_{X \rightarrow Z_{BL} Q}}{g_\rho^{3/2} M_X^2} \\ \Omega_{\psi_2} h^2 &\simeq \sum_{X=h_{1,2,3,A}} \frac{2.18 \times 10^{27} M_{\psi_2} \Gamma_{X \rightarrow \psi_2 \psi_2}}{g_\rho^{3/2} M_X^2} + 2 Br(Z_{BL} \rightarrow \psi_2 \psi_2) \frac{M_{\psi_2}}{M_{Z_{BL}}} (\Omega_{Z_{BL}} h^2). \end{aligned} \quad (44)$$

All the decay widths needed for the analytical estimates in the above equations have been provided in the Appendix. We have checked carefully that the analytical estimates matches perfectly well with the solution obtained after solving the full differential equations with a maximum deviation of 10%.

C. Thermal and non-thermal distributions

In the left panel (LP) of Fig. 4, we have shown the $\xi_p^2 f_{Z_{BL}}$ with ξ_p^{-3} for the thermal and non-thermal distribution of Z_{BL} . The parameters value taken for generating the LP and right panel (RP) have been mentioned in the caption of Fig. 4. The non-thermal distribution function of Z_{BL} has been derived after solving the Eq. (38) and for the thermal distribution of Z_{BL} we have Maxwell-Boltzmann distribution $f_{Z_{BL}}^T = e^{-\frac{E}{T}}$ where E is the relativistic energy of Z_{BL} and T is the temperature. The green line shows the non-thermal distribution, blue line shows the thermal distribution and the magenta line shows the ratio between them. We can see the ratio $\frac{f_{Z_{BL}}^{NT}}{f_{Z_{BL}}^T}$ is nearly constant for $\xi_p < 1$ after it is exponential suppressed⁴. Therefore, we can consider $f_{Z_{BL}}^{NT} = \kappa(\xi_p) f_{Z_{BL}}^T$ where $\kappa(\xi_p)$ is nearly constant quantity for $\xi_p < 1$. This proportionality makes

³ Defined in appendix as $\xi_p = \left(\frac{g_s(M_{sc}/z)}{g_s(M_{sc}/z_{ini})} \right)^{1/3} \frac{p M_{sc}}{z}$ where z_{ini} is the initial value, p is the amplitude of three momentum

⁴ In Ref. [56] the distribution function for $z \rightarrow \infty$ has been shown analytically which is not useful in our case because our production is around $z \rightarrow 1$ and $z \sim 10^3$ it decays to DM.

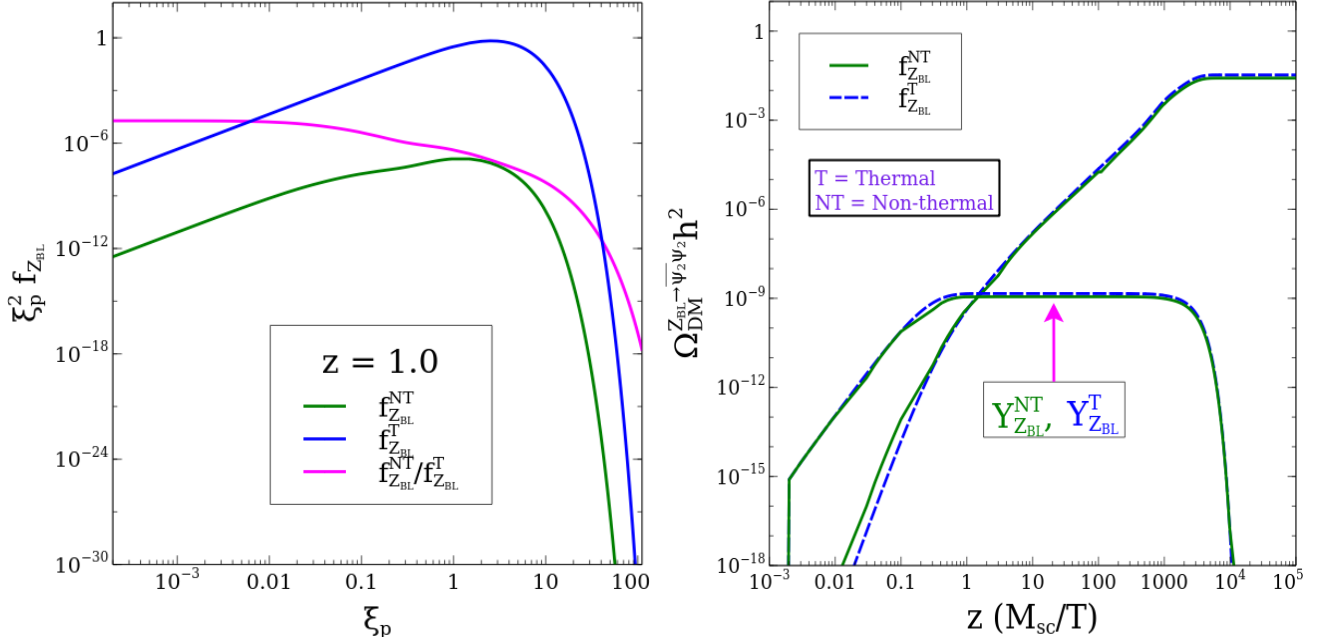


Figure 4: ψ_2 DM production from the Z_{BL} decay by considering thermal and non-thermal distribution function of Z_{BL} . The other parameters have been kept fixed at $M_{h_{2,3}} = 1000$ GeV, $M_A = 1500$ GeV, $\theta_{ij} = 10^{-3}$, $M_{\psi_2} = 1.5$ GeV, $M_{\psi_1} = 200$ GeV, $g_{BL} = 10^{-11}$ and $\tan \beta = 2 \times 10^{-7}$.

sure that the non-thermal decay width of Z_{BL} , $\langle \Gamma_{Z_{BL} \rightarrow BC} \rangle_{NTH}$, as defined in Eq. (41) will be same if we use $f_{Z_{BL}}^{NT}$ or $f_{Z_{BL}}^T$ because for thermal distribution we know $\lim_{z \gg 1} \left(\frac{K_1(z)}{K_2(z)} \right) \rightarrow 1$, i.e. for high z value the numerator and denominator converge to the same values. In the RP of Fig. 4, we have established this statement.

In the RP of Fig. 4, we have shown the comparison of the ψ_2 DM production from the decay of the Z_{BL} after considering its thermal and non-thermal distribution as discussed in the LP. The green solid line has been plotted using the non-thermal distribution, which was derived after solving the Boltzmann equation represented by Eq. (38). Basically, we have computed the distribution function of Z_{BL} and, using it, determined the density of Z_{BL} . On the other hand, the blue dashed line has been generated using the direct decay of BSM Higgs bosons and is independent of the Z_{BL} distribution function. So, in the solid line, we have determined the distribution function of Z_{BL} and, from it, calculated its number density. In contrast, in the blue dashed line, we have directly measured the number density of Z_{BL} without focusing on its distribution function. Since both originate from Higgs decay, they match each other. We observe a strong agreement between the ψ_2 DM production using the thermal and non-thermal distributions of Z_{BL} which is also the finding of the LP. This can be understood by the fact that the Z_{BL} decay is governed by the thermal and non-thermal distribution have the same kind of

effect because of their same kind of distribution with ξ_p with some deviation in the magnitude. As mentioned, there is strong agreement⁵ because, when Z_{BL} decays, the non-thermal distribution of Z_{BL} mimics the thermal distribution value [4, 57]. Therefore, we do not see any deviation in the production of ψ_2 DM. For careful analysis, it is therefore recommended to find the distribution function, but it is very time-consuming because we need to solve two interdependent differential equations simultaneously. In our work, as we obtained the two distributions provides the same output, so we continue our analysis by assuming the thermal distribution of Z_{BL} only to consider its thermal decay width average and the production does not depend on the distribution function, which makes the numerical computation much faster.

D. Line plots

In the left panel of Fig. 5, we have shown the ψ_1 and ψ_2 DM productions by different mechanisms, namely freeze-out [58–60], freeze-in [2, 3], and super-WIMP [61]. The green line shows the production of WIMP-type DM ψ_1 , the blue line shows the Z_{BL} production by the freeze-in mechanism from the decays of $h_{1,2,3}, A$, and the black line shows the freeze-in production of ψ_2 near $z \sim 1$ from the decays of $h_{1,2,3}, A$, as well as super-WIMP production near $z \sim 10^4$ from the decays of Z_{BL} . The magenta line shows the total DM production coming from both ψ_1 and ψ_2 . The grey line shows the Planck 2018 [29] best-fit value for the DM relic density, which coincides with the magenta line. The plot has been generated for BP1, which is also displayed in the caption of the figure. For the subsequent line plots, we have kept the colour coding the same for the different production mechanisms and only changed the line style to indicate the change in parameter values.

In the right panel Fig. 5, we have shown the variation in the DM production for three different values of the gauge coupling g_{BL} . We observe an increment in the Z_{BL} and ψ_2 production as we increase the value of g_{BL} . For the variation of g_{BL} , we have kept the Z_{BL} mass fixed and varied only v_1 and v_2 , which were also kept fixed. The Z_{BL} production is proportional to the square of g_{BL} , which we can see from the blue lines. On the other hand, ψ_2 production is $\propto \frac{1}{v_1^2} \propto g_{BL}^2$, hence we also see an increase in the ψ_2 production as we increase the value of the gauge coupling g_{BL} . The analytical estimates for the production of Z_{BL} and ψ_2 are shown in Eq. (44). We can also observe that due to the change in g_{BL} , the decay lifetime of Z_{BL} also changes, and for higher values of g_{BL} , the decay happens for lower values of z , as seen in the right panel of the figure. Moreover, we see that there is no change in the WIMP DM production, which is because

⁵ We have checked that we have maximal 10% deviation, which can be fixed by iteration during the computation of the differential equation, although this is time-consuming due to multiple iterations, compared to the thermal distribution where we only have a single iteration.

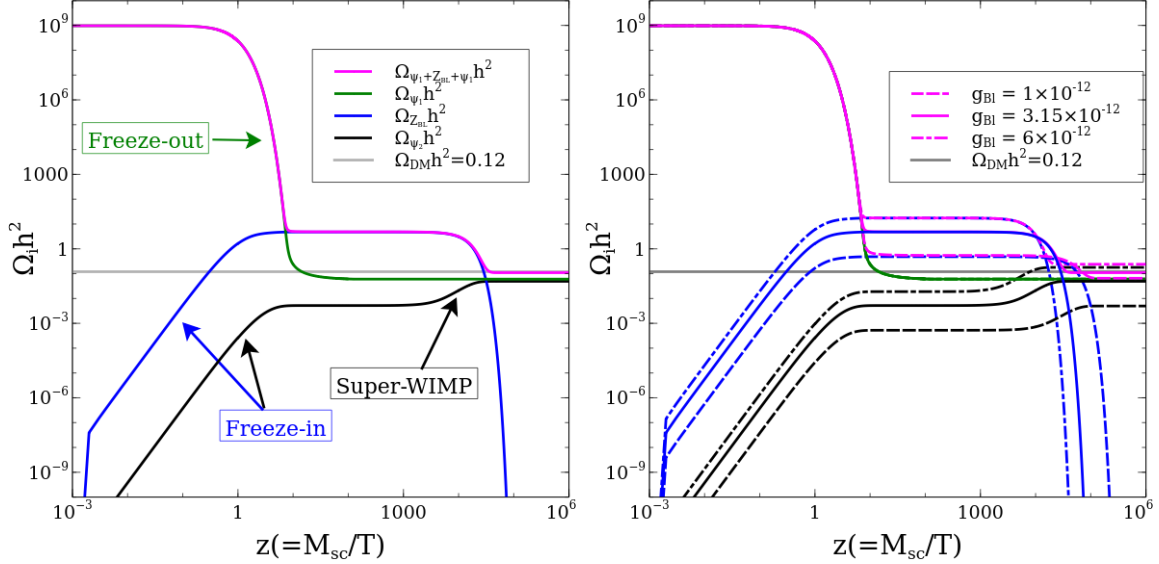


Figure 5: LP shows the $\psi_{1,2}$ DM production by freeze-out, freeze-in and super-WIMP mechanisms whereas RP shows the response of the WIMP and FIMP DM production mechanisms for three different values gauge coupling g_{BL} . The parameters value have been kept fixed at $g_{BL} = 3.15 \times 10^{-12}$, $M_{Z_{BL}} = 24.5$ GeV, $M_{\psi_1} = 408.4$, $M_{\psi_2} = 7.66$ GeV, $\tan \beta = 3.29 \times 10^{-10}$, $M_{h_2} = 131.5$ GeV, $M_{h_3} = 346.6$ GeV, $M_A = 192.5$ GeV and Higgs mixing matrix as $U_{ii} = 1.0$ ($i = 1, 2, 3$), $U_{12} \simeq U_{21} = 0.011$, $U_{13} \simeq U_{31} = 0.003$ and $U_{23} \simeq -U_{32} = 0.0003$. The parameters have been kept fixed for the other line plots as well, unless their variations are explicitly shown.

the production of WIMP DM is proportional to the square of the VEV v_2 , which is unchanged in this case. The total DM density is shown by the magenta points, and we observe that there is variation in the total relic density.

In Fig. 6, we have shown the variation of DM production for three different values of M_{ψ_1} in the left panel and for three different values of M_{ψ_2} in the right panel. In the left panel, we see that there is no effect on the production of the FIMP DM for the variation of M_{ψ_1} , and we observe the opposite scenario for the variation of M_{ψ_2} . In the LP, we can see that for $M_{\psi_1} = 200$ GeV, there is a jump in the WIMP production because $\psi_1 \psi_1 \rightarrow h_3 h_3$ is not allowed kinematically, and $\psi_1 \psi_1 \rightarrow AA$ is phase space suppressed. For the other two values of M_{ψ_1} , we see an increment in the relic density for higher masses due to the reduced effect of phase space suppression, which increases the cross section times velocity and the mass. In the right panel, we can see that the ψ_2 DM relic density increases proportionally with its mass. For the super-WIMP regime, we do not have production of ψ_2 for $M_{\psi_2} = 25.0$ because $Z_{BL} \rightarrow \psi_2 \psi_2$ is kinematically forbidden, but it is kinematically allowed for the other two values of M_{ψ_2} , as seen in the figure. In both plots, we do not observe any effect on the production of Z_{BL} .

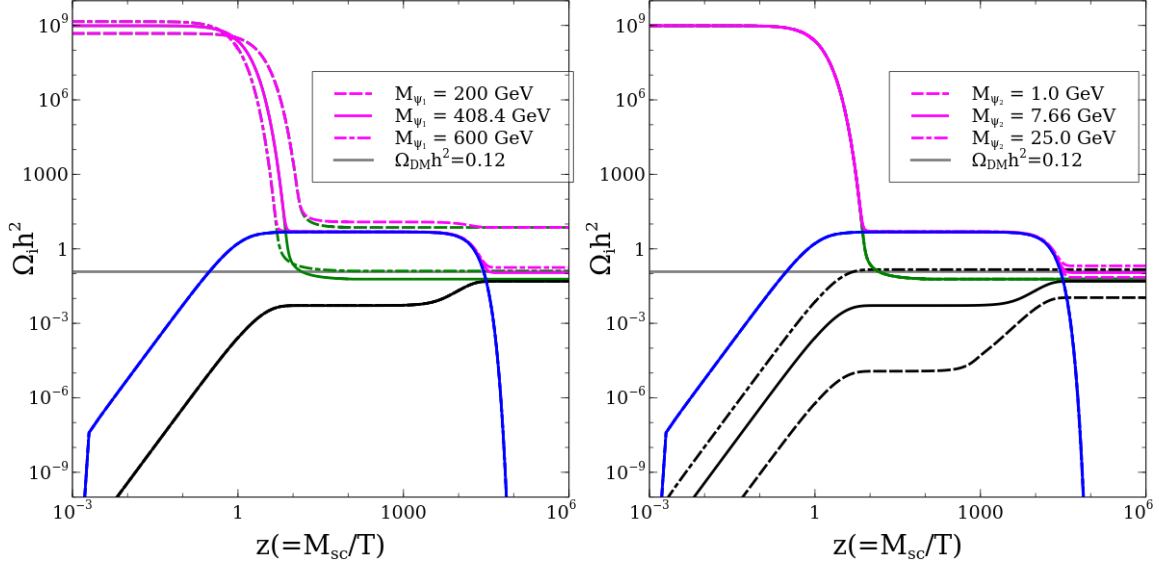


Figure 6: LP and RP shows the WIMP and FIMP type DM relic density variation for three different values of M_{ψ_1} and M_{ψ_2} .

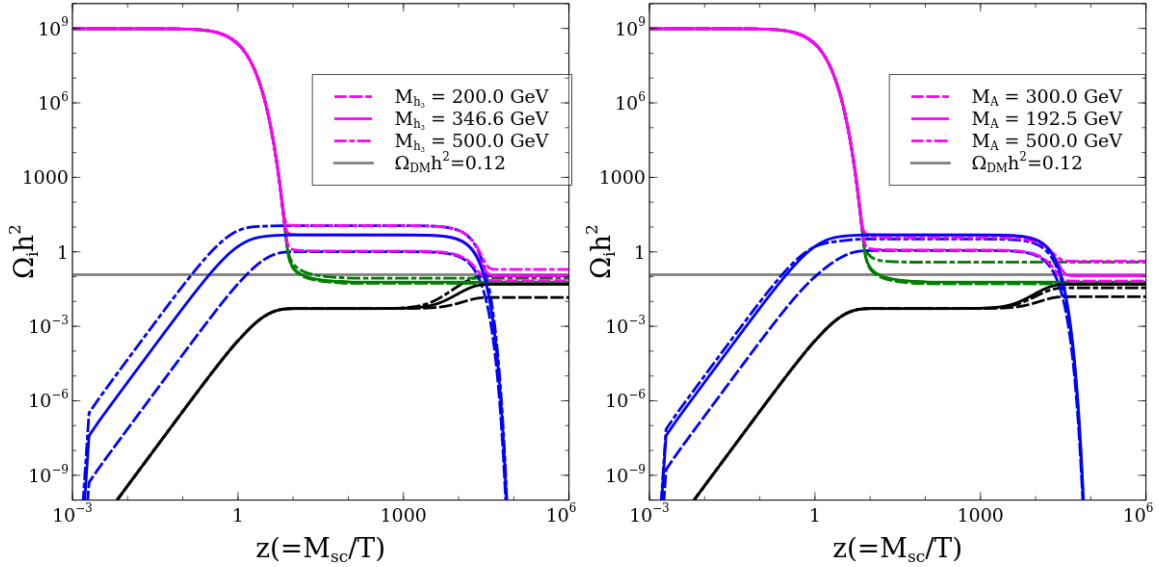


Figure 7: LP (RP) shows the relic density variation for WIMP and FIMP type DM candidates by different mechanisms for three different values of M_{h_2} (M_A).

In the LP and RP of Fig. 7, we have shown the variation in the DM production for three different values of M_{h_3} and M_A , respectively. In both the LP and RP, we can see that there is no effect on the production of ψ_2 for the variation of h_3 and A masses because they are proportional to the Higgs mixing matrix components U_{23} and $\sin \beta$, which are small, as given in the caption

of Fig. 5. Therefore, the mass change does not significantly affect the production, but we have checked that the dominant production of ψ_2 comes from the h_2 decay because it is proportional to U_{22} . In the case of Z_{BL} production, we can see a linear growth with M_{h_3} , but for the RP, it is more complicated. The decay channels $A \rightarrow Z_{BL}h_i$ or $h_i \rightarrow Z_{BL}A$ contribute to Z_{BL} production, depending on the masses. The dominant production mode is $h_3 \rightarrow Z_{BL}A$ (or vice versa), depending on the masses, and other processes are subdominant due to the suppressed mixing. From $M_A = 192.5$ GeV to $M_A = 300$ GeV, there is more phase space suppression, leading to less production of Z_{BL} . However, when we take $M_A = 500$ GeV, the process $A \rightarrow h_3Z_{BL}$ opens up and contributes in a similar amount. This process has more phase space suppression, so it produces slightly less than for $M_A = 192.5$ GeV. For the WIMP-type DM, we observe a small variation for the change in mass, but in the RP, we see a higher jump in the WIMP DM relic density for $M_A = 500$ GeV because the $\psi_1\psi_1 \rightarrow AA$ annihilation mode is kinematically forbidden, which significantly contributes to the DM production for the chosen model parameters.

E. Scattered plots

In generating the scattered plots, we have varied the model parameters in the following range,

$$\begin{aligned}
10^{-4} \leq \theta_{ij} \ (i, j = 1, 2, 3) \leq 10^{-1}, \ 1 \leq (M_{h_{2,3}} - M_{h_1}) \ [\text{GeV}] \leq 10^3, \ 10^{-12} \leq g_{BL} \leq 10^{-8}, \\
1 \leq M_{Z_{BL}} \ [\text{GeV}] \leq 10^3, \ 1 \leq (M_A - (M_{Z_{BL}} + M_{h_1})) \ [\text{GeV}] \leq 10^3, \ 10^{-12} \leq \tan \beta \leq 10^{-6}, \\
1 \leq M_{\psi_1} \ [\text{GeV}] \leq 10^3, \ 1 \leq M_{\psi_2} \ [\text{GeV}] \leq 10^3, \ \theta_L = 0.
\end{aligned} \tag{45}$$

We have chosen the CP-odd Higgs mass M_A within the above range so that it always has two-body decay channel open, avoiding suppression from a three-body decay, which could conflict with the BBN bound. We have demanded that the total DM density for WIMP and FIMP DM candidates from all the mechanisms satisfy the following Planck 5σ range [29],

$$0.1116 \leq (\Omega_{\psi_1} + \Omega_{\psi_2}) h^2 \leq 0.1284. \tag{46}$$

In the LP and RP of Fig. 8, we have shown the scatter plots in the $M_{h_2} - M_A$ and $v_1 - g_{BL}$ planes, respectively. All the points satisfy the bounds listed in section III along with the DM relic density. In the LP, we can see a sharp correlation between the values of M_{h_2} and M_A , and the colour bar shows the different values of the quartic coupling λ_2 . For the potential to be bounded, we need $\lambda_2 > 0$, and the points above the blue line will provide negative values, so those are excluded. Moreover, as we go towards the x-axis, we get higher values of λ_2 , which can be understood from Eq. (27). In the RP, we can see scatter plots in the $v_1 - g_{BL}$ plane, where the colour variation shows the fraction of FIMP DM f_{ψ_2} . We can see from the figure that as we go towards higher values of g_{BL} , we have more production of FIMP-type DM ψ_2 , which can be

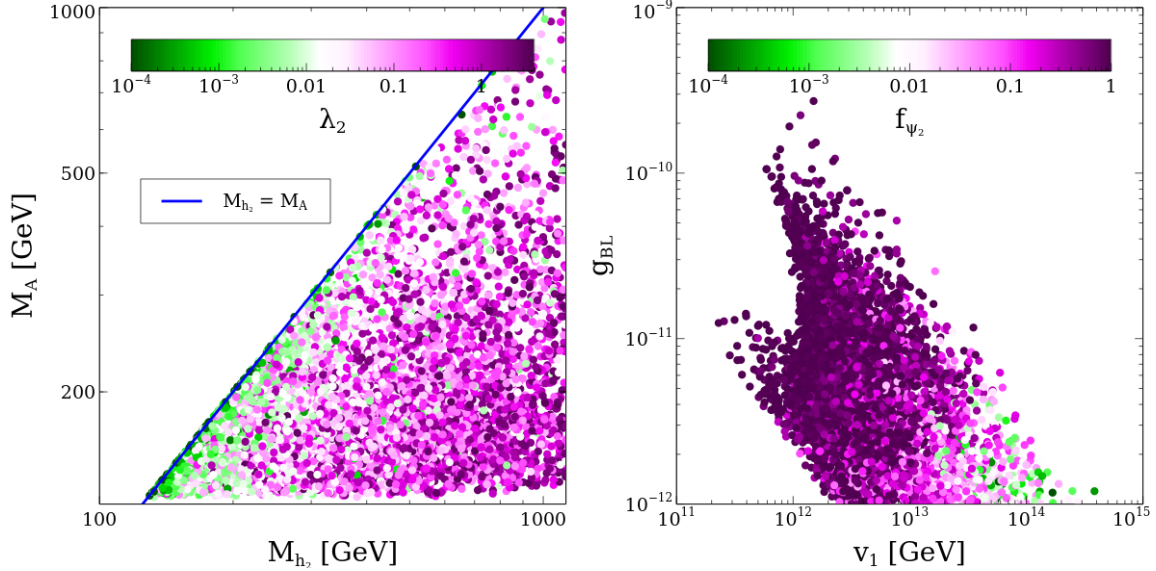


Figure 8: LP and RP shows the scatter plots in the $M_{h_2} - M_A$ and $v_1 - g_{BL}$ planes after satisfying the DM relic density and other constraints mentioned in section III. The colour bar in the LP shows the different values quartic coupling λ_2 whereas the RP shows the fraction of the WIMP DM contribution.

understood from the analytical estimates in Eq. (44). Moreover, as we move along the x-axis, we see a smaller fraction of ψ_2 DM because the production of ψ_2 from the Higgses is inversely proportional to the square of the VEV v_1 . We also see an anti-correlation between v_1 and g_{BL} , which is expected because they appear as a product in the Z_{BL} mass.

In the LP of Fig. 9, we have shown a scatter plot in the $M_{\psi_1} - M_{h_3}$ plane, where the colour bar represents the different values of the fraction of WIMP DM ψ_1 in the total DM density. Near $M_{\psi_1} \sim 62$ GeV, we see a vertical line of points, which are due to the Higgs resonance region. The points are mostly magenta because the cross-section is suppressed by the Higgs mixing angle U_{31} , and hence the dominating contribution to the DM density is from this suppression, rather than the strong effect of resonance. The blue line shows the resonance region between ψ_1 and h_3 . We can see that all the points around the blue line are magenta points and there are no green points. This is because h_3 has a larger decay width, so the resonance effect is mild, which results in the dominating contribution to the DM density. The cyan line represents when $M_{\psi_1} \sim M_{h_3}$. Below the cyan line, the $\bar{\psi}_1\psi_1 \rightarrow h_3h_3, AA$ annihilation modes are open and contribute dominantly, and we can see green points around the cyan line. The region between the blue and cyan lines is mainly due to the DM annihilation to $W^+W^-, ZZ, h_2h_2, h_1h_1$. The main advantage of the region below is that we can achieve DM density for a larger region of the parameter space, which will be pretty safe from direct detection due to the suppression by the mixing angle, which does not have any effect on DM production in this part of the parameter space. In the RP, we can

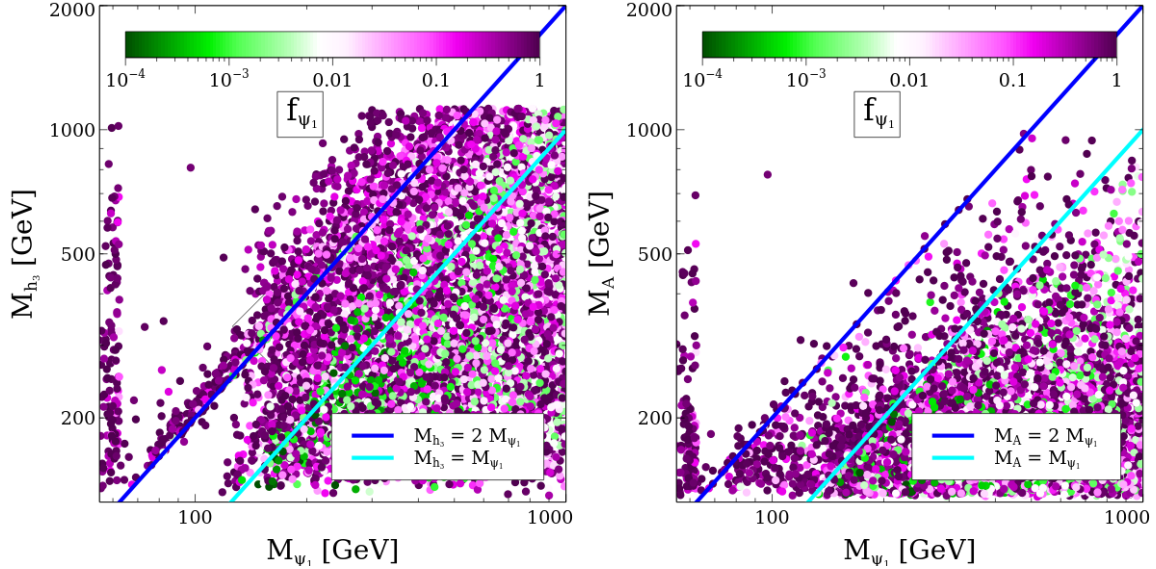


Figure 9: LP shows the allowed region in the $M_{\psi_1} - M_{h_3}$ plane after satisfying all the relevant bounds. In the RP, we have shown the variation in the $M_{\psi_1} - M_A$ plane. In both plots, colour variation shows the fraction of the WIMP DM component.

see the resonance points near half of the SM Higgs mass. We do not see any points beyond the blue line because those points are not allowed by the perturbativity bound coming from the λ_2 quartic coupling, as discussed before. The cyan line represents $M_{\psi_1} \sim M_A$, and below this line, we have the $\bar{\psi}_1 \psi_1 \rightarrow AA$ annihilation mode open. These two plots are important from the present-day severe DD bound because we can choose $M_{\psi_1} > M_{h_3}, M_A$ and satisfy the DM relic density very easily, but at the same time, we can evade the direct detection bound by choosing a smaller mixing angle, which has negligible effect on the DM density.

In the LP of Fig. 10, the scatter plot in the $M_{Z_{BL}} - g_{BL}$ plane is shown, where the colour bar displays the different fractions of FIMP DM ψ_2 contributing to the total DM density. We see a linear relation between $M_{Z_{BL}}$ and g_{BL} , which is expected from the gauge boson mass dependence on g_{BL} , and the width in the correlation arises due to the different values of the VEVs $v_{1,2}$. With the increase of g_{BL} , we see an increment in the ψ_2 DM fraction. The effect of the Z_{BL} mass on the ψ_2 production is not very prominent. The blue line represents the BBN bound, and below that line, Z_{BL} decays after BBN and can alter the successful prediction of BBN. In the RP, we have shown the scatter plot in the $M_{\psi_1} - f_{\psi_1} \sigma_{\psi_1}$ plane, and the colour bar shows the different values of v_2 . The analytical expression for DD is given in Eq. (30). Some parts of the parameter space are already ruled out by the LUX-ZEPLIN 2024 data [1], and the rest will be explored in the near future. As mentioned before, the present model is difficult to rule out by direct detection fully because we can choose a smaller mixing angle between the DM and visible sector,

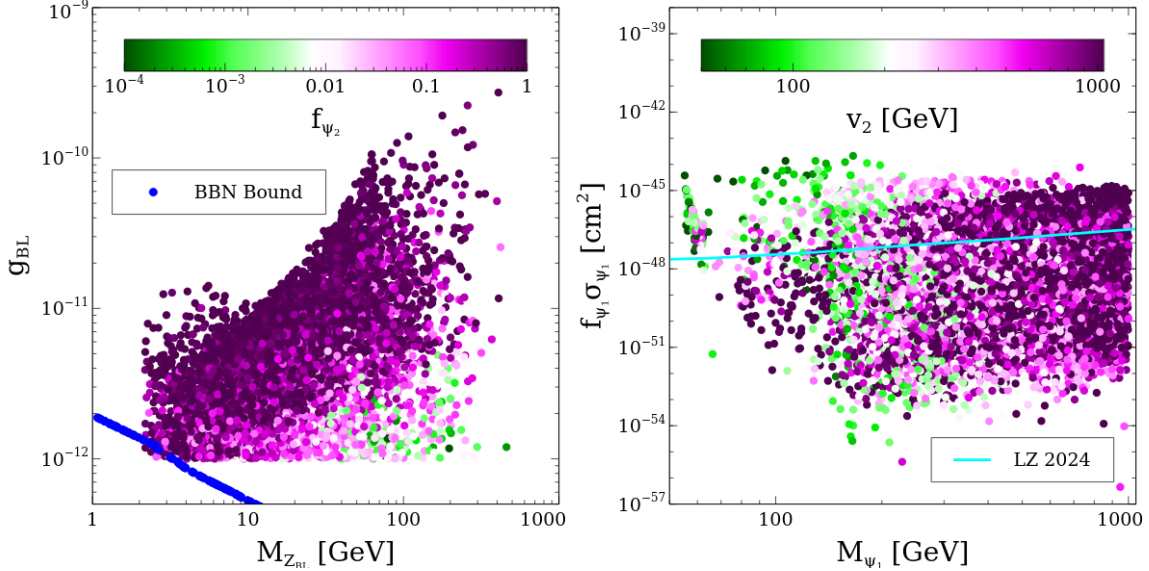


Figure 10: LP shows the scatter plot in the $M_{Z_{BL}} - g_{BL}$ plane and the colour variation represents the fraction of the FIMP DM component. In the RP, we have shown variation in the WIMP DM mass with the SI cross-section where the colour variation shows the different values of VEV v_2 .

which does not affect the DM relic density. Therefore, by choosing a smaller mixing angle, we can evade the bounds without altering the DM density.

In Fig. 11, we have shown scatter plots in the $M_{\psi_1} - f_{\psi_1}^2 \langle \sigma v \rangle_{b\bar{b}}$ and $M_{\psi_1} - f_{\psi_1}^2 \langle \sigma v \rangle_{WW}$ planes. The analytical expressions for indirect detection are shown in Eq. (31). We can see that our DM is fermionic, so from the initial state wave function contraction and averaging over the initial spin, we get an amplitude $\propto (s - 4M_{\psi_1}^2)$, which is $\propto v_{\text{rel}}^2$ in the non-relativistic limit. At present, the DM velocity is taken as $v_{\text{rel}} \sim 10^{-3}$, which makes the indirect detection cross section very small compared to the present-day bound, making it difficult to detect in the near future. In the LP, we have shown the colour variation for the Yukawa coupling value α_{113} , and we can see that a lower value of it contributes to higher values of the ID cross section because we have multiplied by $f_{\psi_1}^2$, which is inversely proportional to the fourth power of the Yukawa coupling α_{113} . In the RP, we have shown in the colour bar the fraction of f_{ψ_1} , and we also see a linear relation with the ID cross-section. Therefore, our present model is very much safe from both direct and indirect detection experiments and is very timely in the context of the recent LUX-ZEPLIN data, which has ruled out a large part of the parameter space.

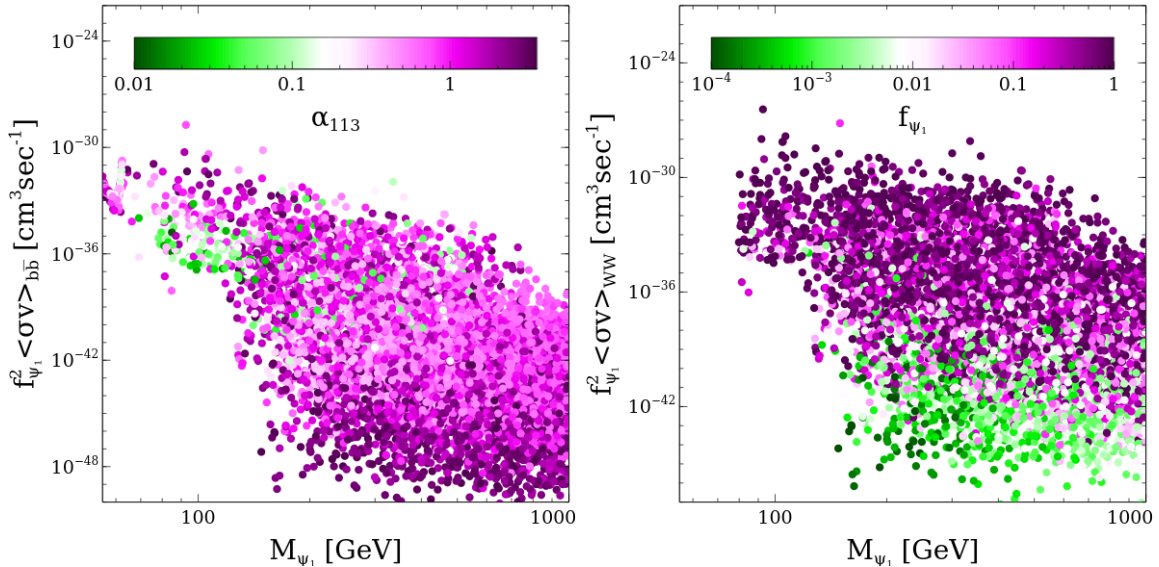


Figure 11: LP and RP show the variation of the WIMP DM mass M_{ψ_1} with the DM annihilation cross section to $b\bar{b}$ and W^+W^- final states. The colour variation in the LP shows the coupling strength α_{113} and the RP shows the fraction of WIMP DM contribution to the total DM density.

V. CONCLUSIONS

In the present work, we have considered the extension of the SM with the $U(1)_{B-L}$ gauge symmetry, but introduced four chiral fermions for gauge anomaly cancellation, instead of three right-handed fermions. Moreover, the scalar sector has been extended by two singlet scalars, whose VEVs provide masses to the extra fermions and the $U(1)_{B-L}$ gauge boson. From the four chiral fermions, we can compose two Dirac fermions, which are candidates for WIMP and FIMP DM in our work. We can take the mixing among the chiral components of the two Dirac fields to zero by introducing two independent Z_2 symmetries for the extra fermions or considering the associated Yukawa couplings to zero. We can achieve many different kinds of possibilities for DM types and productions, but we focused on the WIMP and FIMP DM combination, which could survive even after more severe bounds in the future. We have taken the hierarchical VEVs of the singlet scalars, $v_1 \gg v_2$, to realize the WIMP and FIMP combination at the renormalizable level.

In our model, we considered the mass of the extra gauge boson Z_{BL} in the TeV scale, so we assumed the associated extra gauge coupling in the feeble regime. This makes the extra gauge boson out of equilibrium, so we have computed its non-thermal distribution function for that. However, we found that our analysis does not change even if we consider the thermal distribution for the gauge boson, because the ratio of non-thermal and thermal distributions of the gauge

boson remains fixed for the distribution function with $\xi_p < 1$, and the Z_{BL} number density falls exponentially for larger values of ξ_p . The Z_{BL} gauge boson can be produced dominantly from the decays of SM Higgs and singlet scalars in the early Universe, while the annihilation contributions to the abundance of the Z_{BL} gauge boson can be neglected. We showed that the FIMP DM ψ_2 can be produced from the late decay of Z_{BL} and scalar fields in our model, while the BBN bound is satisfied. The annihilation contributions to the production of FIMP DM can be also neglected.

In the case of WIMP DM, we have focused on the regions of the parameter space where $\psi_1\psi_1 \rightarrow h_i h_i$, AA annihilation modes are active on top of the Higgs resonance region. Since DM mainly annihilates into AA and $h_3 h_3$, we can freely choose the mixing angles that connect the visible and dark sectors. Therefore, a large portion of the parameter space for WIMP DM is still unexplored by existing direct detection experiments but can be probed in future experiments. Moreover, as the WIMP DM is fermionic in nature, the annihilation cross section for WIMP into the SM sector is p -wave suppressed, so it is challenging to probe the WIMP DM by indirect detection experiments. We have shown the allowed regions in various planes for the parameter space after implementing all the relevant constraints.

Moreover, we also showed the possibility of generating neutrino masses by dimension-6 and dimension-7 operators in the effective theory with the $U(1)_{B-L}$ symmetry. These higher-dimensional operators can be realized when the model is extended with three singlet fermions, which are suitably charged under $U(1)_{B-L}$ for gauge anomaly conditions and have the Yukawa interactions with the lepton doublets either by dimension-4 or dimension-5 terms. It would be worthwhile to explore our model further such as alternative production mechanisms for DM and detection prospects at the present and future colliders.

Acknowledgements

The research is supported by Brain Pool program funded by the Ministry of Science and ICT through the National Research Foundation of Korea (RS-2024-00407977) and Basic Science Research Program through the National Research Foundation of Korea (NRF) funded by the Ministry of Education, Science and Technology (NRF-2022R1A2C2003567). For the numerical analysis, we have used the Scientific Compute Cluster at GWDG, the joint data center of Max Planck Society for the Advancement of Science (MPG) and University of Göttingen.

Appendix: Analytical expressions for decay widths and collision terms

If we consider a generic process, $\chi(\tilde{p}) \rightarrow a(\tilde{p}_1) b(\tilde{p}_2)$ (where $\tilde{p} = (E_p, \vec{p})$), then the collision term can be written in the following form [60, 62],

$$\mathcal{C}[f_\chi(p)] = \frac{1}{2E_p} \int \frac{g_a d^3 p_1}{(2\pi)^3 2E_{p_1}} \frac{g_b d^3 p_2}{(2\pi)^3 2E_{p_2}} (2\pi)^4 \delta^4(\tilde{p} - \tilde{p}_1 - \tilde{p}_2) \times \overline{|\mathcal{M}|^2} \times [f_a f_b (1 \pm f_\chi) - f_\chi (1 \pm f_a) (1 \pm f_b)]. \quad (47)$$

Now the full expressions of the collision terms in Eq. (38) are as follows [63, 64],

- $\mathcal{C}^{Z_{BL} \rightarrow all}$: Collision term for the extra gauge boson Z_{BL} total decay takes the the following form,

$$\mathcal{C}^{Z_{BL} \rightarrow all} = -f_{Z_{BL}}(\xi_p) \times \Gamma_{Z_{BL} \rightarrow all} \times \frac{z_{Z_{BL}}}{\sqrt{\xi_p^2 \mathcal{B}(z)^2 + z_{Z_{BL}}^2}}. \quad (48)$$

where $z_{Z_{BL}} = \frac{M_{Z_{BL}}}{T}$, $\mathcal{B}(z) = \left(\frac{g_s(M_{sc}/z)}{g_s(M_{sc}/z_{ini})} \right)^{1/3}$, $\xi_p = \mathcal{B}^{-1}(z) \frac{p}{T}$, $\Gamma_{Z_{BL} \rightarrow all} = \Gamma_{Z_{BL} \rightarrow f\bar{f}} + \Gamma_{Z_{BL} \rightarrow \psi_i \psi_j}$ and the expression for the each decay terms are as follows,

$$\begin{aligned} \Gamma_{Z_{BL} \rightarrow f\bar{f}} &= n_c \frac{M_{Z_{BL}} Q_f^2 g_{BL}^2}{12\pi} \left(1 + \frac{2M_f^2}{M_{Z_{BL}}^2} \right) \sqrt{1 - \frac{4M_f^2}{M_{Z_{BL}}^2}}, \\ \Gamma_{Z_{BL} \rightarrow \psi_i \psi_j} &= \frac{M_{Z_{BL}}}{12\pi} \sqrt{\left[1 - \left(\frac{M_{\psi_1} + M_{\psi_2}}{M_{Z_{BL}}} \right)^2 \right] \left[1 - \left(\frac{M_{\psi_1} - M_{\psi_2}}{M_{Z_{BL}}} \right)^2 \right]} \\ &\times \left[\left(g_{Z_{BL} \psi_i \psi_j}^V \right)^2 \left(1 - \left(\frac{M_{\psi_1} - M_{\psi_2}}{M_{Z_{BL}}} \right)^2 \right) \times \left(1 - \frac{1}{2} \left(\frac{M_{\psi_1} + M_{\psi_2}}{M_{Z_{BL}}} \right)^2 \right) \right. \\ &\left. + \left(g_{Z_{BL} \psi_i \psi_j}^A \right)^2 \left(1 - \left(\frac{M_{\psi_1} + M_{\psi_2}}{M_{Z_{BL}}} \right)^2 \right) \times \left(1 + \frac{1}{2} \left(\frac{M_{\psi_1} - M_{\psi_2}}{M_{Z_{BL}}} \right)^2 \right) \right] \quad (49) \end{aligned}$$

where f is all the SM fermions and Q_f is associated charge under $U(1)_{B-L}$. The coupling of Z_{BL} with the BSM fermions ($\psi_{1,2}$) takes the following form,

$$\begin{aligned} g_{Z_{BL} \psi_1 \psi_1}^V &= \frac{g_{BL}}{6} (1 - 3 \cos^2 \theta_L), & g_{Z_{BL} \psi_1 \psi_1}^A &= \frac{g_{BL}}{6} (3 + 3 \cos^2 \theta_L), \\ g_{Z_{BL} \psi_1 \psi_2}^V &= -\frac{g_{BL}}{3} \sin^2 \theta_L, & g_{Z_{BL} \psi_1 \psi_2}^A &= \frac{g_{BL}}{3} \sin^2 \theta_L, \\ g_{Z_{BL} \psi_2 \psi_2}^V &= \frac{g_{BL}}{6} (1 - 3 \sin^2 \theta_L), & g_{Z_{BL} \psi_1 \psi_1}^A &= \frac{g_{BL}}{6} (3 + 3 \sin^2 \theta_L). \end{aligned} \quad (50)$$

- $\mathcal{C}^{X \rightarrow Z_{BL} Y}$: The collision term for the production of the extra gauge boson Z_{BL} via the

decay of the BSM scalars h_i , A is expressed as follows,

$$\begin{aligned} \mathcal{C}^{X \rightarrow Z_{BL} Y} &= \frac{z}{16\pi M_{sc}} \frac{\mathcal{B}^{-1}(z)}{\xi_p \sqrt{\xi_p^2 \mathcal{B}(z)^2 + \left(\frac{M_{Z_{BL}} z}{M_{sc}}\right)^2}} \frac{|M|_{X \rightarrow Z_{BL} Y}^2}{g_{Z_{BL}}} \\ &\times \left(e^{-\sqrt{(\xi_k^{\min})^2 \mathcal{B}(z)^2 + \left(\frac{M_{h_2} z}{M_{sc}}\right)^2}} - e^{-\sqrt{(\xi_k^{\max})^2 \mathcal{B}(z)^2 + \left(\frac{M_{h_2} z}{M_{sc}}\right)^2}} \right). \end{aligned} \quad (51)$$

where $g_{Z_{BL}} = 3$, the squared decay amplitude, $|M|_{X \rightarrow Z_{BL} Y}^2$, is without any average over initial and final states, and the symmetric factor automatically cancels when we multiply by the same final states, $Z_{BL} Z_{BL}$. The other relevant quantities for producing the DM density are defined below,

$$\begin{aligned} |M|_{h_i \rightarrow Z_{BL} Z_{BL}}^2 &= g_{h_i Z_{BL} Z_{BL}}^2 \left(2 + \frac{(M_{h_2}^2 - 2M_{Z_{BL}}^2)^2}{4M_{Z_{BL}}^4} \right), \\ |M|_{P \rightarrow Z_{BL} Q}^2 &= g_{P Z_{BL} Q}^2 (M_P^2 - (M_Q - M_{Z_{BL}})^2) (M_P^2 - (M_Q + M_{Z_{BL}})^2) \text{ with } P, Q = h_i, A, \\ g_{h_i Z_{BL} Z_{BL}} &= 2g_{BL}^2 (U_{2i} v_2 + 4U_{3i} v_1), \quad g_{A Z_{BL} h_i} = g_{BL} (2U_{3i} \cos \beta + U_{2i} \sin \beta), \quad i = 1, 2, 3, \\ \xi_k^{\min}(\xi_p, z) &= \frac{M_{sc}}{2\mathcal{B}(z) z M_{Z_{BL}}} \left| \eta(\xi_p, z) - \frac{\mathcal{B}(z) \times M_{h_2}^2}{M_{Z_{BL}} \times M_{sc}} \xi_p z \right|, \\ \xi_k^{\max}(\xi_p, z) &= \frac{M_{sc}}{2\mathcal{B}(z) z M_{Z_{BL}}} \left(\eta(\xi_p, z) + \frac{\mathcal{B}(z) \times M_{h_2}^2}{M_{Z_{BL}} \times M_{sc}} \xi_p z \right), \\ \eta(\xi_p, z) &= \left(\frac{M_{h_2} z}{M_{sc}} \right) \sqrt{\left[\left(\frac{M_X}{M_{Z_{BL}}} + 1 \right)^2 - \left(\frac{M_Y}{M_{Z_{BL}}} \right)^2 \right] \left[\left(1 - \frac{M_{Z_{BL}}}{M_X} \right)^2 - \left(\frac{M_{Z_{BL}}}{M_X} \right)^2 \right]} \\ &\times \sqrt{\xi_p^2 \mathcal{B}(z)^2 + \left(\frac{M_{Z_{BL}} z}{M_{sc}} \right)^2}. \end{aligned} \quad (52)$$

Here, the above expressions match with those in Ref. [57] for the same final state particles.

- The other relevant decay widths, which have been used in our study, are as follows.

– Decay width for $h_i \rightarrow Z_{BL} Z_{BL}$ can be expressed as follows,

$$\Gamma_{h_i \rightarrow Z_{BL} Z_{BL}} = \frac{M_{h_i}^3 g_{h_i Z_{BL} Z_{BL}}^2}{128\pi M_{Z_{BL}}^4} \sqrt{1 - \frac{4M_{Z_{BL}}^2}{M_{h_i}^2}} \left(1 - \frac{4M_{Z_{BL}}^2}{M_{h_i}^2} + \frac{12M_{Z_{BL}}^4}{M_{h_i}^4} \right) \quad (53)$$

where the vertex factors $g_{h_i Z_{BL} Z_{BL}}$ are given in Eq. (52).

- The decay width for $X \rightarrow Z_{BL}Y$, where $X, Y = h_i, A$ depending on masses, can be expressed as

$$\Gamma_{X \rightarrow Z_{BL}Y} = \frac{g_{XZ_{BL}Y}^2 M_X^3}{16\pi M_{Z_{BL}}^2} \left[1 - \left(\frac{M_{Z_{BL}} + M_Y}{M_X} \right)^2 \right]^{3/2} \left[1 - \left(\frac{M_{Z_{BL}} - M_Y}{M_X} \right)^2 \right]^{3/2} \quad (54)$$

where the coupling $g_{XZ_{BL}Y}$ is defined in Eq. (52).

- The decay width of h_i to BSM fermions can be expressed as,

$$\Gamma_{h_i \rightarrow \psi_j \psi_j} = \frac{M_{h_i} \alpha_{jji}^2}{16\pi} \left(1 - \frac{4M_{\psi_i}^2}{M_{h_i}^2} \right)^{3/2}, \quad (55)$$

where the coupling constants α_{jji} ($j = 1, 2$ and $i = 1, 2, 3$) are given in Eq. (20).

- The decay width for the $A \rightarrow \psi_i \psi_i$, $i = 1, 2$, can be expressed as

$$\Gamma_{A \rightarrow \psi_i \psi_i} = \frac{\alpha_{iiA}^2 M_A}{8\pi} \sqrt{1 - \frac{4M_{\psi_i}^2}{M_A^2}} \quad (56)$$

where the vertex factors are given in Eq. (20).

-
- [1] J. Aalbers *et al.* [LZ Collaboration], [arXiv:2410.17036 [hep-ex]].
 - [2] J. McDonald, Phys. Rev. Lett. **88**, 091304 (2002) doi:10.1103/PhysRevLett.88.091304 [arXiv:hep-ph/0106249 [hep-ph]].
 - [3] L. J. Hall, K. Jedamzik, J. March-Russell and S. M. West, JHEP **03**, 080 (2010) doi:10.1007/JHEP03(2010)080 [arXiv:0911.1120 [hep-ph]].
 - [4] W. Abdallah, S. Choubey and S. Khan, JHEP **06**, 095 (2019) doi:10.1007/JHEP06(2019)095 [arXiv:1904.10015 [hep-ph]].
 - [5] F. Costa, S. Khan and J. Kim, JHEP **06**, 026 (2022) doi:10.1007/JHEP06(2022)026 [arXiv:2202.13126 [hep-ph]].
 - [6] L. Covi and S. Khan, JCAP **09**, 064 (2022) doi:10.1088/1475-7516/2022/09/064 [arXiv:2205.10150 [hep-ph]].
 - [7] G. Bélanger, S. Choubey, R. M. Godbole, S. Khan, M. Mitra and A. Roy, JHEP **11**, 133 (2022) doi:10.1007/JHEP11(2022)133 [arXiv:2208.00849 [hep-ph]].
 - [8] F. Costa, S. Khan and J. Kim, JHEP **12**, 165 (2022) doi:10.1007/JHEP12(2022)165 [arXiv:2209.13653 [hep-ph]].
 - [9] S. Khan, J. Kim, J. Kim and P. Ko, [arXiv:2409.07851 [hep-ph]].

- [10] C. A. J. O'Hare, Phys. Rev. Lett. **127**, no.25, 251802 (2021) doi:10.1103/PhysRevLett.127.251802 [arXiv:2109.03116 [hep-ph]].
- [11] C. Cosme, F. Costa and O. Lebedev, Phys. Rev. D **109**, no.7, 075038 (2024) doi:10.1103/PhysRevD.109.075038 [arXiv:2306.13061 [hep-ph]].
- [12] J. Silva-Malpartida, N. Bernal, J. Jones-Pérez and R. A. Lineros, JCAP **09**, 015 (2023) doi:10.1088/1475-7516/2023/09/015 [arXiv:2306.14943 [hep-ph]].
- [13] G. Arcadi, F. Costa, A. Goudelis and O. Lebedev, JHEP **07**, 044 (2024) doi:10.1007/JHEP07(2024)044 [arXiv:2405.03760 [hep-ph]].
- [14] H. M. Lee, M. Park and V. Sanz, [arXiv:2412.07850 [hep-ph]].
- [15] A. Biswas, S. Choubey and S. Khan, JHEP **08**, 114 (2016) doi:10.1007/JHEP08(2016)114 [arXiv:1604.06566 [hep-ph]].
- [16] R. N. Mohapatra and R. E. Marshak, Phys. Rev. Lett. **44**, 1316-1319 (1980) [erratum: Phys. Rev. Lett. **44**, 1643 (1980)] doi:10.1103/PhysRevLett.44.1316
- [17] H. M. Georgi, S. L. Glashow and S. Nussinov, Nucl. Phys. B **193**, 297-316 (1981) doi:10.1016/0550-3213(81)90336-9
- [18] C. Wetterich, Nucl. Phys. B **187**, 343-375 (1981) doi:10.1016/0550-3213(81)90279-0
- [19] M. Lindner, D. Schmidt and T. Schwetz, Phys. Lett. B **705**, 324-330 (2011) doi:10.1016/j.physletb.2011.10.022 [arXiv:1105.4626 [hep-ph]].
- [20] N. Okada and O. Seto, Phys. Rev. D **82**, 023507 (2010) doi:10.1103/PhysRevD.82.023507 [arXiv:1002.2525 [hep-ph]].
- [21] S. Patra, W. Rodejohann and C. E. Yaguna, JHEP **09**, 076 (2016) doi:10.1007/JHEP09(2016)076 [arXiv:1607.04029 [hep-ph]].
- [22] A. Biswas, S. Choubey and S. Khan, JHEP **08**, 062 (2018) doi:10.1007/JHEP08(2018)062 [arXiv:1805.00568 [hep-ph]].
- [23] J. Kim, S. S. Kim, H. M. Lee and R. Padhan, Phys. Lett. B **861** (2025), 139243 doi:10.1016/j.physletb.2025.139243 [arXiv:2407.13595 [hep-ph]].
- [24] W. Konetschny and W. Kummer, Phys. Lett. B **70**, 433-435 (1977) doi:10.1016/0370-2693(77)90407-5
- [25] J. Schechter and J. W. F. Valle, Phys. Rev. D **22**, 2227 (1980) doi:10.1103/PhysRevD.22.2227
- [26] E. J. Chun, S. Khan, S. Mandal, M. Mitra and S. Shil, Phys. Rev. D **101**, no.7, 075008 (2020) doi:10.1103/PhysRevD.101.075008 [arXiv:1911.00971 [hep-ph]].
- [27] P. S. B. Dev, S. Khan, M. Mitra and S. K. Rai, Phys. Rev. D **99**, no.11, 115015 (2019) doi:10.1103/PhysRevD.99.115015 [arXiv:1903.01431 [hep-ph]].
- [28] I. Esteban, M. C. Gonzalez-Garcia, M. Maltoni, I. Martinez-Soler, J. P. Pinheiro and T. Schwetz, [arXiv:2410.05380 [hep-ph]].
- [29] N. Aghanim *et al.* [Planck], Astron. Astrophys. **641**, A6 (2020) [erratum: Astron. Astrophys. **652**,

- C4 (2021)] doi:10.1051/0004-6361/201833910 [arXiv:1807.06209 [astro-ph.CO]].
- [30] J. M. Cline, K. Kainulainen, P. Scott and C. Weniger, Phys. Rev. D **88**, 055025 (2013) [erratum: Phys. Rev. D **92**, no.3, 039906 (2015)] doi:10.1103/PhysRevD.88.055025 [arXiv:1306.4710 [hep-ph]].
- [31] G. Belanger, F. Boudjema, A. Pukhov and A. Semenov, Comput. Phys. Commun. **180**, 747-767 (2009) doi:10.1016/j.cpc.2008.11.019 [arXiv:0803.2360 [hep-ph]].
- [32] M. L. Ahnen *et al.* [MAGIC and Fermi-LAT], JCAP **02**, 039 (2016) doi:10.1088/1475-7516/2016/02/039 [arXiv:1601.06590 [astro-ph.HE]].
- [33] A. Acharyya *et al.* [CTA], JCAP **01**, 057 (2021) doi:10.1088/1475-7516/2021/01/057 [arXiv:2007.16129 [astro-ph.HE]].
- [34] Y. Heo, D. W. Jung and J. S. Lee, Phys. Rev. D **110**, no.1, 013003 (2024) doi:10.1103/PhysRevD.110.013003 [arXiv:2402.02822 [hep-ph]].
- [35] G. Aad *et al.* [ATLAS], Nature **607**, no.7917, 52-59 (2022) [erratum: Nature **612**, no.7941, E24 (2022)] doi:10.1038/s41586-022-04893-w [arXiv:2207.00092 [hep-ex]].
- [36] A. Tumasyan *et al.* [CMS], Nature **607**, no.7917, 60-68 (2022) [erratum: Nature **623**, no.7985, E4 (2023)] doi:10.1038/s41586-022-04892-x [arXiv:2207.00043 [hep-ex]].
- [37] G. Aad *et al.* [ATLAS and CMS], JHEP **08**, 045 (2016) doi:10.1007/JHEP08(2016)045 [arXiv:1606.02266 [hep-ex]].
- [38] K. Herner [CDF and D0], Nucl. Part. Phys. Proc. **273-275**, 852-856 (2016) doi:10.1016/j.nuclphysbps.2015.09.131
- [39] A. M. Sirunyan *et al.* [CMS], Phys. Lett. B **793**, 520-551 (2019) doi:10.1016/j.physletb.2019.04.025 [arXiv:1809.05937 [hep-ex]].
- [40] A. Tumasyan *et al.* [CMS], JHEP **11**, 153 (2021) doi:10.1007/JHEP11(2021)153 [arXiv:2107.13021 [hep-ex]].
- [41] A. M. Sirunyan *et al.* [CMS], Eur. Phys. J. C **81**, no.1, 13 (2021) [erratum: Eur. Phys. J. C **81**, no.4, 333 (2021)] doi:10.1140/epjc/s10052-020-08739-5 [arXiv:2008.04735 [hep-ex]].
- [42] M. Carena, A. Daleo, B. A. Dobrescu and T. M. P. Tait, Phys. Rev. D **70**, 093009 (2004) doi:10.1103/PhysRevD.70.093009 [arXiv:hep-ph/0408098 [hep-ph]].
- [43] G. Cacciapaglia, C. Csaki, G. Marandella and A. Strumia, Phys. Rev. D **74**, 033011 (2006) doi:10.1103/PhysRevD.74.033011 [arXiv:hep-ph/0604111 [hep-ph]].
- [44] S. Chatrchyan *et al.* [CMS], Phys. Lett. B **720**, 63-82 (2013) doi:10.1016/j.physletb.2013.02.003 [arXiv:1212.6175 [hep-ex]].
- [45] G. Aad *et al.* [ATLAS], Phys. Rev. D **90**, no.5, 052005 (2014) doi:10.1103/PhysRevD.90.052005 [arXiv:1405.4123 [hep-ex]].
- [46] M. Kawasaki, K. Kohri, T. Moroi and Y. Takaesu, Phys. Rev. D **97**, no.2, 023502 (2018) doi:10.1103/PhysRevD.97.023502 [arXiv:1709.01211 [hep-ph]].

- [47] W. Grimus, L. Lavoura, O. M. Ogreid and P. Osland, Nucl. Phys. B **801**, 81-96 (2008) doi:10.1016/j.nuclphysb.2008.04.019 [arXiv:0802.4353 [hep-ph]].
- [48] T. A. Aaltonen *et al.* [CDF and D0], Phys. Rev. D **88**, no.5, 052018 (2013) doi:10.1103/PhysRevD.88.052018 [arXiv:1307.7627 [hep-ex]].
- [49] M. Aaboud *et al.* [ATLAS], Eur. Phys. J. C **78**, no.2, 110 (2018) [erratum: Eur. Phys. J. C **78**, no.11, 898 (2018)] doi:10.1140/epjc/s10052-017-5475-4 [arXiv:1701.07240 [hep-ex]].
- [50] R. Aaij *et al.* [LHCb], JHEP **01**, 036 (2022) doi:10.1007/JHEP01(2022)036 [arXiv:2109.01113 [hep-ex]].
- [51] T. A. Aaltonen *et al.* [CDF], Phys. Rev. D **89**, no.7, 072003 (2014) doi:10.1103/PhysRevD.89.072003 [arXiv:1311.0894 [hep-ex]].
- [52] G. Belanger, F. Boudjema, A. Pukhov and A. Semenov, Comput. Phys. Commun. **149**, 103-120 (2002) doi:10.1016/S0010-4655(02)00596-9 [arXiv:hep-ph/0112278 [hep-ph]].
- [53] A. Alloul, N. D. Christensen, C. Degrande, C. Duhr and B. Fuks, Comput. Phys. Commun. **185**, 2250-2300 (2014) doi:10.1016/j.cpc.2014.04.012 [arXiv:1310.1921 [hep-ph]].
- [54] A. Belyaev, N. D. Christensen and A. Pukhov, Comput. Phys. Commun. **184**, 1729-1769 (2013) doi:10.1016/j.cpc.2013.01.014 [arXiv:1207.6082 [hep-ph]].
- [55] J. Edsjo and P. Gondolo, Phys. Rev. D **56**, 1879-1894 (1997) doi:10.1103/PhysRevD.56.1879 [arXiv:hep-ph/9704361 [hep-ph]].
- [56] Q. Decant, J. Heisig, D. C. Hooper and L. Lopez-Honorez, JCAP **03**, 041 (2022) doi:10.1088/1475-7516/2022/03/041 [arXiv:2111.09321 [astro-ph.CO]].
- [57] A. Biswas, S. Choubey, L. Covi and S. Khan, JCAP **02**, 002 (2018) doi:10.1088/1475-7516/2018/02/002 [arXiv:1711.00553 [hep-ph]].
- [58] E. W. Kolb and K. A. Olive, Phys. Rev. D **33**, 1202 (1986) [erratum: Phys. Rev. D **34**, 2531 (1986)] doi:10.1103/PhysRevD.33.1202
- [59] M. Srednicki, R. Watkins and K. A. Olive, Nucl. Phys. B **310**, 693 (1988) doi:10.1016/0550-3213(88)90099-5
- [60] P. Gondolo and G. Gelmini, Nucl. Phys. B **360**, 145-179 (1991) doi:10.1016/0550-3213(91)90438-4
- [61] L. Covi, J. E. Kim and L. Roszkowski, Phys. Rev. Lett. **82**, 4180-4183 (1999) doi:10.1103/PhysRevLett.82.4180 [arXiv:hep-ph/9905212 [hep-ph]].
- [62] E. W. Kolb, Front. Phys. **69**, 1-547 (1990) Taylor and Francis, 2019, ISBN 978-0-429-49286-0, 978-0-201-62674-2 doi:10.1201/9780429492860
- [63] J. König, A. Merle and M. Totzauer, JCAP **11**, 038 (2016) doi:10.1088/1475-7516/2016/11/038 [arXiv:1609.01289 [hep-ph]].
- [64] A. Biswas and A. Gupta, JCAP **03**, 033 (2017) doi:10.1088/1475-7516/2017/03/033 [arXiv:1612.02793 [hep-ph]].